National Library of Canada
Bibliothèque nationale du Canada

Canadian Theses Service
Service des thèses canadiennes

Ottawa, Canada
K1A 0N4

NOTICE

The quality of this microform is heavily dependent upon the quality of the original thesis submitted for microfilming. Every effort has been made to ensure the highest quality of reproduction possible.

If pages are missing, contact the university which granted the degree.

Some pages may have indistinct print especially if the original pages were typed with a poor typewriter ribbon or if the university sent us an inferior photocopy.

Reproduction in full or in part of this microform is governed by the Canadian Copyright Act, R.S.C. 1970, c. C-30, and subsequent amendments.

AVIS

La qualité de cette microforme dépend grandement de la qualité de la thèse soumise au microfilmage. Nous avons tout fait pour assurer une qualité supérieure de reproduction.

S'il manque des pages, veuillez communiquer avec l'université qui a conféré le grade.

La qualité d'impression de certaines pages peut laisser à désirer, surtout si les pages originales ont été dactylographiées à l'aide d'un ruban usé ou si l'université nous a fait parvenir une photocopie de qualité inférieure.

La reproduction, même partielle, de cette microforme est soumise à la Loi canadienne sur le droit d'auteur, SRC 1970, c. C-30, et ses amendements subséquents.

NL-339 (r. 88/04) c

Canada

UNIVERSITY OF ALBERTA

DYNAMIC RESPONSE OF KIPP & ZONEN CM-5 PYRANOMETER - ITS MEASUREMENT, ANALYSIS AND HIGH ORDER ERROR CORRECTION

by

BING SHEN

A THESIS

SUBMITTED TO THE FACULTY OF GRADUATE STUDIES AND RESEARCH

IN PARTIAL FULFILLMENT OF THE REQUIREMENTS FOR THE DEGREE OF

MASTER OF SCIENCE

DEPARTMENT OF ELECTRICAL ENGINEERING

EDMONTON, ALBERTA

SPRING 1992

National Library of Canada
Bibliothèque nationale du Canada

Canadian Theses Service
Service des thèses canadiennes

Ottawa, Canada
K1A 0N4

The author has granted an irrevocable non-exclusive licence allowing the National Library of Canada to reproduce, loan, distribute or sell copies of his/her thesis by any means and in any form or format, making this thesis available to interested persons.

L'auteur a accordé une licence irrévocable et non exclusive permettant à la Bibliothèque nationale du Canada de reproduire, prêter, distribuer ou vendre des copies de sa thèse de quelque manière et sous quelque forme que ce soit pour mettre des exemplaires de cette thèse à la disposition des personnes intéressées.

The author retains ownership of the copyright in his/her thesis. Neither the thesis nor substantial extracts from it may be printed or otherwise reproduced without his/her permission.

L'auteur conserve la propriété du droit d'auteur qui protège sa thèse. Ni la thèse ni des extraits substantiels de celle-ci ne doivent être imprimés ou autrement reproduits sans son autorisation.

ISBN 0-315-73123-0

Canada

UNIVERSITY OF ALBERTA

RELEASE FORM

NAME OF AUTHOR: *BING SHEN*

TITLE OF THESIS: *DYNAMIC RESPONSE OF KIPP & ZONEN CM-5 PYRANOMETER — ITS MEASUREMENT, ANALYSIS AND HIGH ORDER ERROR CORRECTION*

DEGREE: *MASTER OF SCIENCE*

YEAR THIS DEGREE GRANTED: *SPRING 1992*

PERMISSION IS HEREBY GRANTED TO THE UNIVERSITY OF ALBERTA LIBRARY TO REPRODUCE SINGLE COPIES OF THIS THESIS AND TO LEND OR SELL SUCH COPIES FOR PRIVATE, SCHOLARLY OR SCIENTIFIC RESEARCH PURPOSES ONLY.

THE AUTHOR RESERVES OTHER PUBLICATION RIGHTS, AND NEITHER THE THESIS NOR EXTENSIVE EXTRACTS FROM IT MAY BE PRINTED OR OTHERWISE REPRODUCED WITHOUT THE AUTHOR'S WRITTEN PERMISSION.

(signed) 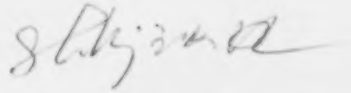

Bing Shen

Beiyuan Dayuan

Anwai, Beijing

P.R. China

Date: Jan 7, 1992

UNIVERSITY OF ALBERTA

FACULTY OF GRADUATE STUDIES AND RESEARCH

THE UNDERSIGNED CERTIFY THEY HAVE READ, AND RECOMMEND TO THE FACULTY OF GRADUATE STUDIES AND RESEARCH FOR ACCEPTANCE, A THESIS ENTITLED **DYNAMIC RESPONSE OF KIPP & ZONEN CM-5 PYRANOMETER - ITS MEASUREMENT, ANALYSIS AND HIGH ORDER ERROR CORRECTION** SUBMITTED BY **BING SHEN** IN PARTIAL FULFILLMENT OF THE REQUIREMENTS FOR THE DEGREE OF **MASTER OF SCIENCE**.

A.M. Robinson

.....

Dr. A.M. Robinson (Supervisor)

J.N. McMullin

.....

Dr. J.N. McMullin

Gerald W. Sadler

.....

Prof. G.W. Sadler

Date: Dec. 18, 1991

Dedicated

To my wife Li Nan

ABSTRACT

Thermal pyranometers and pyrheliometers are the most frequently used instruments for solar radiation measurement. Due to the thermal inertia of their sensors, the output signals are unable to follow exactly a rapid radiation change. For instantaneous solar radiation measurements, correction for the time-response-error becomes necessary.

Brinkworth and Hughes [4, 5] proposed an electronic compensation circuit which could accelerate the response of thermal radiation instruments. However, their hardware scheme, of which the accuracy depends largely on the electronic element quality and the environmental conditions, may introduce changes in the instrument's calibration constants. A software scheme has been developed by Suehrcke *et al.* [6] by analyzing a linear sensor model using heat transfer theory. Suehrcke's approach may be questioned when the measured instrumental response to step function radiation varies significantly from a single exponential function, which is one of his important assumptions.

In this work, the response of Kipp & Zonen CM-5 thermal pyranometers to a step radiation change was measured. It was observed that the pyranometer output varied significantly from a single exponential function of time. Using a multi-exponential function to fit the

experimental data, the two dominant exponential components of the signal, as well as their time constants, were extracted.

A thermal model of the pyranometer has been developed, whose response displays the observed time behavior. The model lead to the derivation of a transient function describing the relationship between the pyranometer output and the radiation input.

In order to determine an unknown parameter in the transient function, sinusoidal response of the same pyranometer was examined. Based on the experimentally determined transient function, a second order correction scheme (SOC) was developed to correct the second order time response error. As the time response error occurs, SOC has demonstrated definite improvement over both the original thermal sensor readings and the first order correction scheme proposed by Suehrcke *et al.* [6].

ACKNOWLEDGEMENTS

The author is indebted to his supervisor Dr. A.M. Robinson who has given his patience, constant encouragement and guidance throughout this research work. Special appreciation should be extended to Dr. P.R. Smy and R.P.W. Lawson for their concerns and support. The author wishes to thank the Department of Electrical Engineering for providing the opportunity and financial assistance.

Technical assistance from Mr. R. Haley has been an immense contribution and is greatly appreciated. Without him, the simple and ingenious experimental setups would be not possible.

The author also wishes to express his heartfelt gratitude to Prof. W. Joerg and Mr. Yanmin Li who have always been a constant source of support throughout this research work.

Finally, a well-deserved expression of appreciation goes to the author's wife and family members, and to all his teachers for their invaluable contributions.

TABLE OF CONTENTS

Chapter	Page
1. INTRODUCTION	1
1.1 Solar radiation sensor	1
1.2 Time response error	3
1.3 Error compensation	5
2. RESPONSE MODEL OF THERMAL PYRANOMETER	12
2.1 Suehrcke's model	12
2.2 Double thin plate model	15
2.2.1 Transient function	15
2.2.2 Step and sinusoidal response	19
3. STEP RESPONSE OF KIPP & ZONEN CM-5 PYRANOMETERS	25
3.1 Instrumentation	25
3.2 Experimental results and analysis	26
3.3 Response to impulse radiation	28
3.4 Correction for measurement of step radiation	30
4. SINUSOIDAL RESPONSE OF KIPP & ZONEN CM-5 PYRANOMETER	40
4.1 Experimental setup	40
4.2 Measurement and analysis	41
4.3 Conclusions	44

5. TIME RESPONSE ERROR CORRECTION 52

5.1 Introduction 52

5.2 Numerical differentiation 52

5.2.1 3-point collocation 53

5.2.2 Data smoothing 54

5.3 Time response error correction 57

5.3.1 Runge-Kutta method 57

5.3.2 Initial condition and partial instability 58

5.3.3 Error correction for experimentally generated radiation 59

5.3.4 Error correction for solar radiation measurement 62

6. CONCLUSIONS 68

6.1 Summary of contributions 68

6.2 Limitations and future work suggestions 69

REFERENCES 72

APPENDIX A. PASCAL PROGRAM FOR DETERMINING THE BEST FIT FREQUENCY OF A SINUSOIDAL FUNCTION 75

APPENDIX B. PASCAL PROGRAM FOR 2ND ORDER TIME RESPONSE ERROR CORRECTION OF THERMAL PYRANOMETER 82

LIST OF TABLES

Table	Page
3.1 The value of τ's of six pyranometers	33

LIST OF FIGURES

Figure		Page
1.1	Photovoltaic radiation sensor	8
1.2	Spectral sensitivity of PV sensor and typical solar radiation spectrum	9
1.3	Time response error of thermal pyranometer	10
1.4	Thermal shock response of pyranometers	11
2.1	Single plate thermal pyranometer model	22
2.2	Sinusoidal response of single plate model	23
2.3	Double plate thermal pyranometer model	24
3.1	Experimental setup for step response measurement	34
3.2	Pyranometer response to a downward step of radiation	35
3.3	Extraction of τ_1 signal from the original signal	36
3.4	Pyranometer response to a pulse radiation	37
3.5	Comparison between the pulse and the step response	38
3.6	First and second order corrections to the pyranometer readings for a downward step of radiation	39
4.1	Experimental setup for the sinusoidal response measurement	45
4.2	Shape of the sinusoidal modulator template	46
4.3	Sinusoidal response of the thermal and photovoltaic	

pyranometers 47

4.4 Flowchart of frequency (ω) optimization program 48

4.5 Lag time of sinusoidal response between the pyranometers 50

4.6 Attenuation of sinusoidal response of the thermal pyranometer 51

5.1 Demonstration of how smaller Δt can increase the differentiation error 63

5.2 Step response correction using 3-point collocation method 64

5.3 Response time FOC and SOC to an arbitrary radiation signal 65

5.4 Demonstration of FOC and SOC in actual solar radiation measurement 67

1. INTRODUCTION

Renewed interest in solar energy has developed as a result of today's energy crises and environmental problems. The design and analysis of solar energy utilization present unique problems, due to the intermittent and diffuse nature of the resource and the high initial expenditures of the conversion system. These characteristics have made it important to accurately predict the process performance and consequently generated activity in both measurements of the process input (solar radiation) and in the application of modeling techniques. Until now, most of the modeling activities have been based on hourly or daily solar radiation values. But recent solar radiation research has demonstrated the need for instantaneous solar radiation values [3]. As the sampling period approaches the order of radiation sensor response, however, time response errors may be encountered in the radiation measurement.

1.1 Solar radiation sensor

Depending on the principle on which they are based, radiation sensors may be broadly classified as photoelectric (or photovoltaic) and thermoelectric sensors.

As its name implies, a photoelectric sensor makes a conversion between photons of light energy and electrical signal. This procedure, as

shown in Figure 1.1, is made possible by a PN junction which collects the electron-hole pairs excited by incident radiation photons. The photoelectric sensor provides a simple, inexpensive radiation instrument that yields a strong output signal without external power. A further and important advantage is that the photoelectric detector, of which the response time is estimated to be about 10 μs [1], is virtually instantaneously activated by the discrete events of the incident photon flux. However, not every photon in Figure 1.1 is able to stimulate an electron-hole pair to the conduction band since the energy of the sun's photons is so spread out that only a few have an energy exactly equal to the band gap of silicon. Insufficiently energetic photons contribute nothing to the output current. A spectral sensitivity curve for a silicon sensor and a typical solar radiation spectrum is shown in Figure 1.2. This effect makes the photovoltaic sensor suffer from accuracy problems since the spectrum of clear sky solar radiation is different from the cloudy sky radiation spectrum [19].

A thermoelectric sensor, based on the principle of converting the incident radiant energy into heat, can overcome the spectral sensitivity problem. In the sensor, a blackened (or partly black and partly white) receiver which is not spectrally selective over the visible and near infrared band is used to provide an indication, or a quantitative reading which is proportional to the incident amount of energy. The energy absorbed by the receiver gives rise to a temperature difference ΔT in the receiver, which depends on its thermal properties. The temperature difference in turn gives rise to a

heat flow i_h, and there is a thermal resistance R_h to this flow which is analogous to electrical resistance. In fact, in the case of stationary heat flow, a law similar to Ohm's law may be employed:

$$\Delta T = i_h R_h \tag{1.1}$$

As the thermal equilibrium state is reached, the heat flow i_h should respond only to the incident radiation. While the temperature difference ΔT may be measured accurately by either thermocouple or thermopiles, the evaluation of R_h is very complicated and an absolute determination is almost impossible. The determination of i_h is therefore not a simple matter. However, when R_h can be maintained at a constant value, measurements of radiation are possible and may be carried out with satisfactory accuracy. Because of their signal's direct connection with the total energy absorbed and their nonselective feature to the spectral distribution of the energy, thermoelectric sensors have conventionally played a major role in solar radiation instruments.

1.2 Time response error

As has already been mentioned, the thermal equilibrium status of the thermoelectric sensor has to be reached before any correct readings could be obtained. If not, a time response error could occur due to the imbalance between the internal thermal flow and the incident radiant energy.

The time response of the instruments depend on their operation principles, mechanical structures and thermal properties. General time response discussions on a group of such instruments, or pyranometers, used to measure global solar radiation, can be found in L.F. van Wely and G.J. van den Brink's work [2], where the step response of instruments is used to represent their dynamic characteristics. According to their measurements, the settling time needed by the pyranometer signals to reach the final stable value after the onset of step input, ranged from 60 s to 180 s for different types of pyranometers. In another words, thermal pyranometers yield erroneous readings for at least 60 s after a sudden step radiation change.

Further investigations of the time effect of the pyranometer was performed by H. Suehrcke [3] who conducted a comparison between a thermal Kipp & Zonen CM-10 and a photovoltaic pyranometer. Both pyranometers were placed under a clear-cloudy sky and their outputs plotted, as shown in Figure 1.3. Due to its instantaneous time response, the photovoltaic pyranometer can be assumed to give the true solar radiation recording. Figure 1.3 shows that the signals from the two pyranometers are almost identical during the time 13:51:10 to 13:51:25 and 13:52:00 to 13:52:35 (or from 13:49:45 to 13:50:38), corresponding to cloudy sky conditions and clear sky conditions respectively. That is because that both cloudy and clear conditions had brought a internal thermal equilibrium status to the thermal radiation sensor and the readings of the pyranometer would consequently represent the true radiation value. But as a clear-cloudy or cloudy-clear transition occurs, at about 13:50:45, and 13:51:40 in

Figure 1.3, the thermal pyranometer CM-10 sensor cannot follow the rapidly changing radiation and yields erroneous readings for approximately 20 s. It is also seen that the thickness and density variation associated with the cloud movement, from 13:52:37 to 13:53:00, is still too fast to be caught accurately by the thermal pyranometer.

Thus thermal radiation sensors, measuring instantaneous solar radiation, can yield inaccurate readings due to their thermal inertia as the radiation changes rapidly.

1.3 Error compensation

Some efforts have been made to compensate or to correct the time response error [4, 5, 6]. An electronic compensation circuit was proposed by Brinkworth and Hughes [4, 5] to accelerate the dynamic response of thermal radiation instruments. When the compensating circuit is used with the Kipp and Zonen pyranometers, the response to a step change in radiation is substantially completed in about 2.3 s [5], much faster than that obtained by van Wely *et al.* [2]. However, this hardware compensation scheme, of which the accuracy depends largely on the precision of the electronics and the environmental conditions, may introduce changes in the instrument's calibration constants. Based on the analysis of a linear sensor model using heat transfer theory, Suehrcke *et al.* have developed a software correction scheme [6], which is based on the instrument response to a step function of radiation being described by a single exponential

function. The software scheme, simple and free of modification to the measurement circuit, takes the advantages from both the modern techniques for data handling and the reliabilities of conventional instruments.

However, careful investigations [2, 7, 8, 13, 14] of the thermal pyranometers have indicated that their dynamic responses can not be described by simple first order behavior, i.e. the step response can't be fit to a single exponential function. In addition to this, the thermal shock measurements of Wardle and Barton [10], as shown in Figure 1.4, suggest that the output signal of a darkened pyranometer, after the ambient temperature drops abruptly, doesn't change exponentially. Instead, the signal goes back to the level before the thermal shock occurs. This phenomenon can't be explained by Suehrcke's single plate model of the thermal pyranometer. Similar results were obtained by van den Brink [11]. Van Wely and van den Brink [2] suggest that pyranometers in general have multiple time constants, caused by the inertia of the sensor, the net infra-red radiation between the inner dome and sensor, and a change in the temperature of the instrument housing. Apparently only the first order time response error is corrected by Suehrcke's scheme and the high order error correction is the purpose of this work.

This thesis begins with a brief introduction on the solar radiation measurement sensors followed by the model development for the thermal pyranometer in Chapter 2, where a relationship (transient function) between the radiant input and sensor output is derived. Chapter 3

presents the investigation of the multiple time constant phenomenon of Kipp & Zonen CM-5 pyranometers, subject to an experimentally-generated step change of radiation. Chapter 4 introduces the sinusoidal response of the pyranometer, the experimental realization of the measurement and the determination of an unknown constant in the transient function. A time response error correction scheme based on the transient function is discussed and demonstrated in Chapter 5, and conclusions are drawn in Chapter 6.

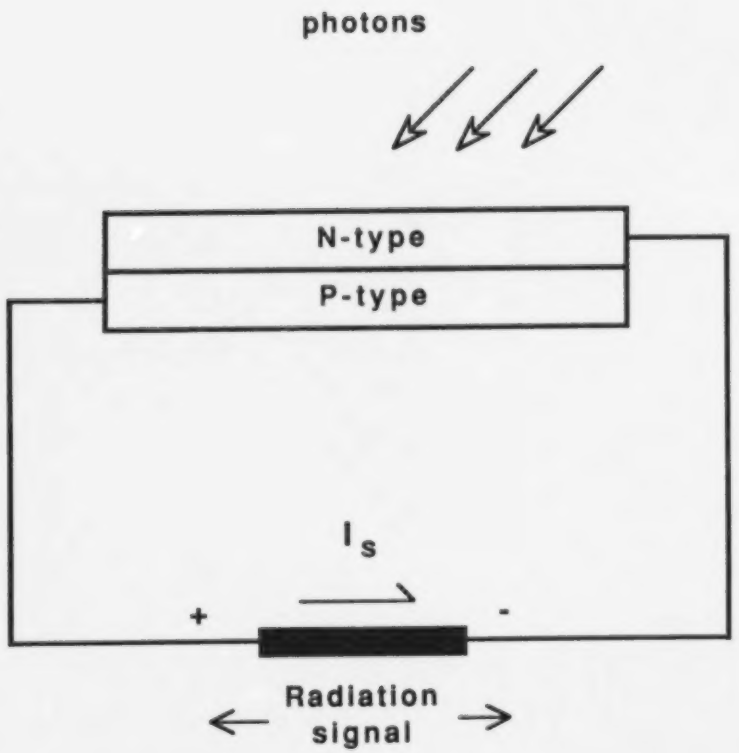

Figure 1.1 Photovoltaic radiation sensor.

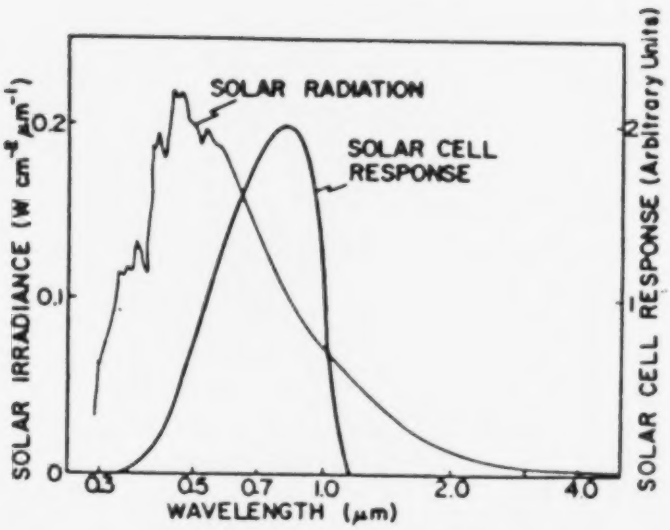

Figure 1.2 Spectral sensitivity of PV sensor and typical solar radiation spectrum. Adapted from Coulson [1].

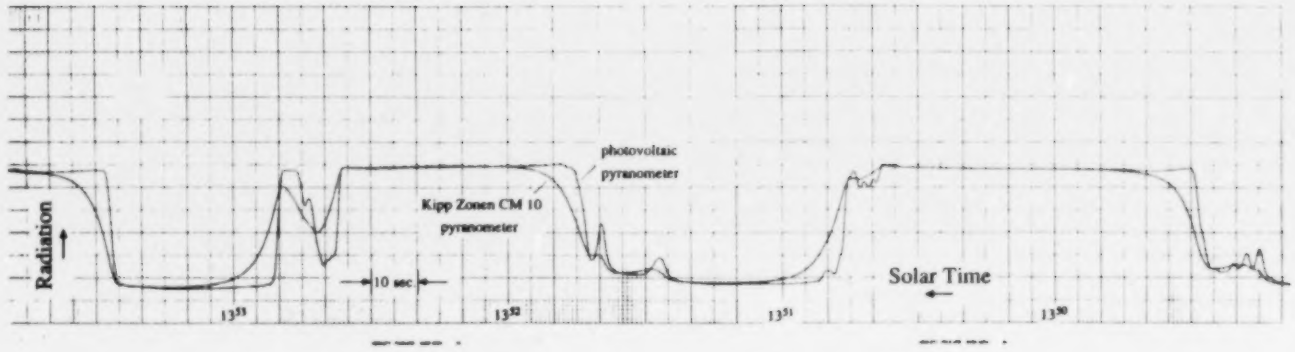

Figure 1.3 Time response error of thermal pyranometer. Adapted from Suehrcke [3].

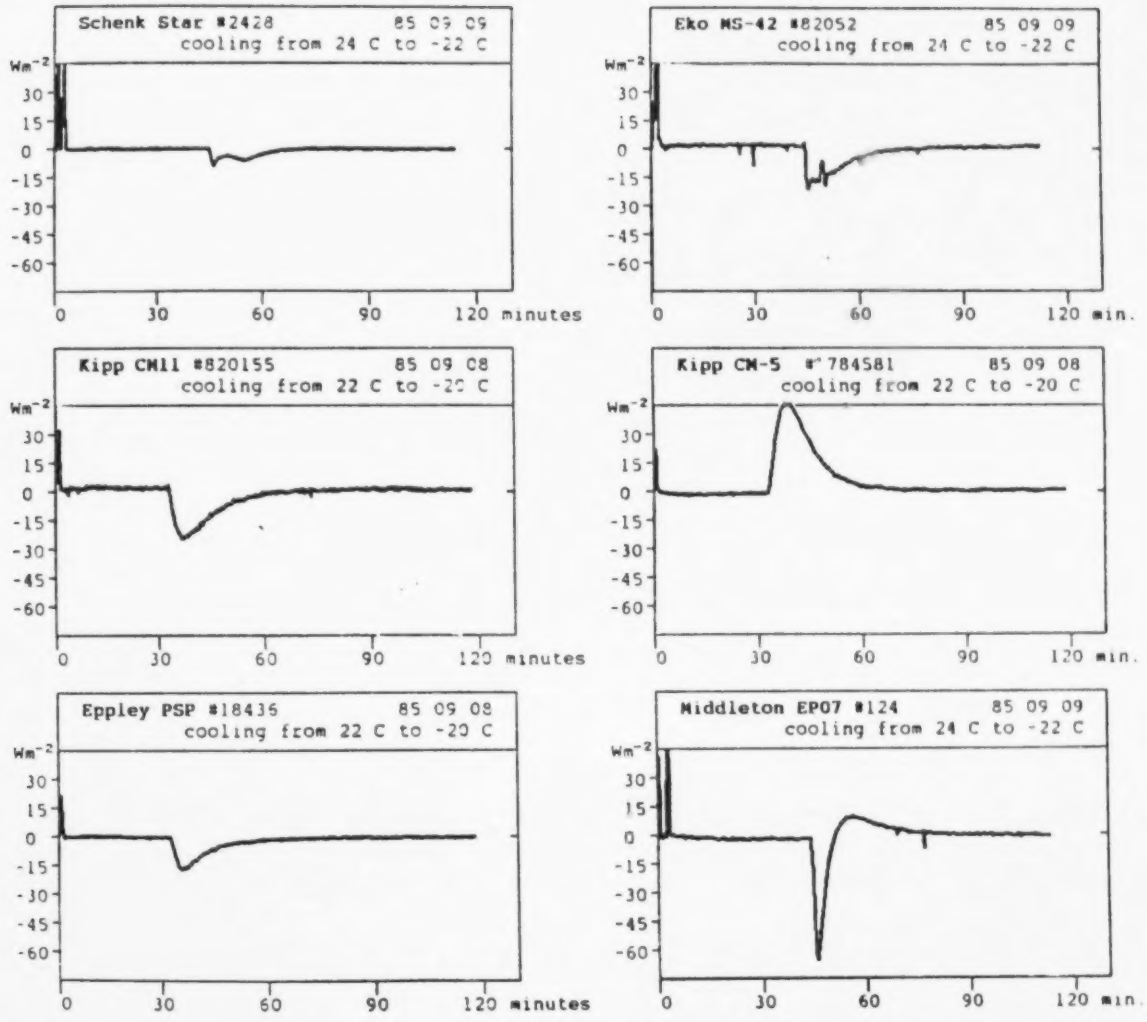

Figure 1.4 Thermal shock response of pyranometers.

Adapted from Wardle *et al.* [10].

2. RESPONSE MODEL OF THERMAL PYRANOMETER

2.1 Suehrcke's model

To correct the time response error, Suehrcke *et al.* [6] have developed a single plate thermal pyranometer model, which has well demonstrated the first order behavior of the instrument. In Suehrcke's analysis, the thermal radiation sensor response is equalized to the temperature response of a thin plate that tries to reach its equilibrium temperature when it is exposed to changing radiation, as shown schematically in Figure 2.1. Assuming that the incident radiation intensity on the pyranometer is G(t) and using the first law of thermodynamics, the equation that governs the response of the sensor can be formulated as:

$$(MC)\frac{dT(t)}{dt} = (\mathcal{T}\alpha)G(t)-U(T(t)-T_a) \qquad (2.1)$$

where (MC) is the effective sensor heat capacitance per unit area, T denotes the sensor plate temperature, $(\mathcal{T}\alpha)$ the glass dome transmittance and sensor surface absorptance product, U the overall heat loss coefficient per unit area, and T_a the ambient temperature. Let T_s be the equilibrium temperature that is reached by the sensor when dT/dt=0. For this case Equation (2.1) yields the relation between the plate temperature and the incident radiation:

$$G = \frac{U}{(\mathcal{T}\alpha)} (T_s - T_a) \tag{2.2}$$

Assuming a linear relation between plate temperature and radiometer reading, the radiation indicated by the sensor, G_i, can be expressed in the same form as Equation (2.2):

$$G_i(t) = \frac{U}{(\mathcal{T}\alpha)} (T(t) - T_a) \tag{2.3}$$

Using Equation (2.3) in Equation (2.1) yields:

$$G(t) = G_i(t) + \tau \frac{dG_i(t)}{dt} \tag{2.4}$$

where $\tau=(MC)/U$ is the time constant of the sensor. Equation (2.4) is used directly, in Suehrcke's compensation for time response error, to correct the erroneous radiation instrument output $G_i(t)$ to the true radiation $G(t)$, provided that the instrument's time constant and the first derivative of the indicated radiation are known.

For some special functions of incident radiation $G(t)$, Equation (2.4) may be solved analytically. Here two special forms of radiation fluctuation are selected for analysis: a step change and a periodic or sinusoidal change.

Consider first a step change in radiation, described by $G(t)=G_0$ for $t \leq t_0$ and $G(t)=G_1$ for $t>t_0$. The instrument response, determined by solving Equation (2.4) analytically, is:

$$G_i(t)=(G_0-G_1)\exp(-(t-t_0)/\tau)+G_1 \qquad (2.5)$$

where $t>t_0$.

Another interesting time response of the pyranometer is its sinusoidal response, sometimes referred as the frequency response. For radiation oscillations described by $G(t)=K \sin(\omega t)$*, where ω represents the angular frequency of oscillation in radians per unit time and the amplitude K is constant, Equation (2.4) becomes:

$$K \sin(\omega t) = G_i(t) + \tau \frac{dG_i(t)}{dt} \qquad (2.6)$$

which is a linear, first-order differential equation having the solution:

$$G_i(t)=C \exp(-t/\tau)+K (1+(\omega\tau)^2)^{-1/2} \sin(\omega t-\arctan \omega\tau) \qquad (2.7)$$

where C is a constant that may be evaluated by the initial condition.

Reference to Figure 2.2 shows that the signal from the sensor is reduced in amplitude to the value αK, where $\alpha=(1+(\omega\tau)^2)^{-1/2}$ is the attenuation factor. $G_i(t)$ also lags behind $G(t)$ by the amount

---

* This is the simplified expression. In fact, radiation oscillation should be described by $G(t)=K \sin(\omega t)+K'$, where $K'>K>0$, since radiation value can't be negative.

$\arctan(\omega\tau)$, once sufficient time has elapsed so that the initial transient has died away. The lag expressed as a phase angle in radians can be converted to time units if divided by ω. To a close approximation, the time (t_L) that the sensor lags behind the incident radiation change is the time constant τ because $\arctan(\omega\tau) \cong \omega\tau$ when $\omega\tau$ is small.

Suehrcke's model is simple and may be applied to the basic understanding and the first-degree correction for the time response error [6]. But for higher order corrections, further investigation on the sensor model will be needed.

2.2 Double thin plate model

In general, a thermal radiation sensor produces a signal by a temperature difference due to a differential absorption of radiation, between either a black and a white surface, two black surfaces, or a blackened surface and the base or housing of the instrument [9]. Thus the single thin plate of Suehrcke's sensor model may not be sufficient to describe the sensor behavior.

2.2.1 Transient function

More realistically, our thermal model of the pyranometer, shown schematically in Figure 2.3, is composed of two thin plates 1 and 2, each with an effective heat capacitance (MC), and overall heat loss coefficient (U). T_a is the ambient temperature. Plate 1, with

absorptance α, is exposed to the radiation G(t) under a glass dome of transmittance $\mathcal{T}$. The pyranometer output is proportional to the difference between the temperatures of the plates.

Using the first law of thermodynamics, the model behavior can be depicted by the following equations:

$$(M_1C_1)\frac{dT_1(t)}{dt} = (\mathcal{T}\alpha)\ G(t)-U_{1a}\ [T_1(t)-T_a]-U_{12}\ [T_1(t)-T_2(t)] \qquad (2.8)$$

$$(M_2C_2)\frac{dT_2(t)}{dt} = U_{12}\ [T_1(t)-T_2(t)]-U_{2a}\ [T_2(t)-T_a] \qquad (2.9)$$

where (M_iC_i) and T_i are the effective heat capacitance and temperature of plate i respectively, 'a' denotes the ambient medium (air), and U_{ij} represents the overall heat loss coefficient from medium i to j.

From (2.8),

$$T_2(t) = \frac{M_1C_1}{U_{12}}\ \frac{dT_1(t)}{dt} + \frac{U_{1a}+U_{12}}{U_{12}}\ T_1(t)- \frac{\alpha\mathcal{T}}{U_{12}}\ G(t)- \frac{U_{1a}}{U_{12}}\ T_a \qquad (2.10)$$

Inserting (2.10) and its derivative into (2.9) results in:

$$\ddot{T}_1(t)+\frac{(M_1C_1)(U_{2a}+U_{12})+(M_2C_2)(U_{1a}+U_{12})}{(M_1C_1)(M_2C_2)}\dot{T}_1(t)+\frac{U_{1a}U_{12}+U_{1a}U_{2a}+U_{2a}U_{12}}{(M_1C_1)(M_2C_2)}\times$$

$$(T_1(t)-T_a) = \frac{\alpha\mathcal{I}}{M_1C_1}\dot{G}(t)+\frac{(\alpha\mathcal{I})(U_{12}+U_{2a})}{(M_1C_1)(M_2C_2)}G(t) \qquad (2.11)$$

Also from (2.9),

$$T_1(t) = \frac{M_2C_2}{U_{12}}\frac{dT_2(t)}{dt}+\frac{U_{12}+U_{2a}}{U_{12}}T_2(t)-\frac{U_{2a}T_a}{U_{12}} \qquad (2.12)$$

Inserting (2.12) into (2.8) yields:

$$\ddot{T}_2(t)+\frac{(M_1C_1)(U_{2a}+U_{12})+(M_2C_2)(U_{1a}+U_{12})}{(M_1C_1)(M_2C_2)}\dot{T}_2(t)+\frac{U_{1a}U_{12}+U_{1a}U_{2a}+U_{2a}U_{12}}{(M_1C_1)(M_2C_2)}\times$$

$$(T_2(t)-T_a) = \frac{U_{12}(\alpha\mathcal{I})}{(M_1C_1)(M_2C_2)}G(t) \qquad (2.13)$$

Subtracting (2.13) from (2.11) obtains:

$$\ddot{\Delta T}(t)+\frac{(M_1C_1)(U_{2a}+U_{12})+(M_2C_2)(U_{1a}+U_{12})}{(M_1C_1)(M_2C_2)}\dot{\Delta T}(t)+\frac{U_{1a}U_{12}+U_{1a}U_{2a}+U_{2a}U_{12}}{(M_1C_1)(M_2C_2)}\times$$

$$\Delta T(t) = \frac{\alpha \mathcal{J}}{M_1 C_1} \dot{G}(t) + \frac{U_{2a}(\alpha \mathcal{J})}{(M_1 C_1)(M_2 C_2)} G(t) \qquad (2.14)$$

where $\Delta T(t) = T_1(t) - T_2(t)$.

Let ΔT_s be the static equilibrium temperature difference when $\ddot{\Delta T}(t) = \dot{\Delta T}(t) = \dot{G}(t) = 0$. Equation (2.14) then yields the relation between ΔT_s and the radiation value indicated by the pyranometer G_i which, under this circumstance, equals to the incident radiation:

$$G_i = G = \frac{U_{12}U_{1a} + U_{1a}U_{2a} + U_{2a}U_{12}}{(\alpha \mathcal{J})\, U_{2a}} \Delta T_s \qquad (2.15)$$

It is assumed that the pyranometer output $G_i(t)$, for time-varying radiation $G(t)$, has the same form as (2.15) so that:

$$G_i(t) = \frac{U_{12}U_{1a} + U_{1a}U_{2a} + U_{2a}U_{12}}{(\alpha \mathcal{J})\, U_{2a}} \Delta T(t) \qquad (2.16)$$

Using (2.16) in (2.14) yields:

$$C_0 \dot{G}(t) + G(t) = C_1 \ddot{G}_i(t) + C_2 \dot{G}_i(t) + G_i(t) \qquad (2.17)$$

where

$$C_0 = M_2C_2 / U_{2a}$$

$$C_1 = (M_1C_1)(M_2C_2)/(U_{1a}U_{12} + U_{1a}U_{2a} + U_{2a}U_{12})$$

$$C_2 = (M_1C_1(U_{2a} + U_{12}) + M_2C_2(U_{1a} + U_{12}))/(U_{1a}U_{12} + U_{1a}U_{2a} + U_{2a}U_{12})$$

Equation (2.17) is the transient function used to describe the behavior of the pyranometer.

2.2.2 Step and sinusoidal response

Equation (2.17) may also be analytically solved for a step or a periodic (sinusoidal) change of incident radiation G(t).

Solution of (2.17) for a step function of radiation, described as before, at $t=t_0$ yields:

$$G_i(t) = A \exp(-(t-t_0)/\tau_1) + B \exp(-(t-t_0)/\tau_2) + G_1 \qquad (2.18)$$

where A and B are constants related to the initial conditions, namely $A+B=G_0-G_1$. Unlike (2.5), the step response of the double thin plate model is composed of two exponential components, with time constants τ_1 and τ_2, which are determined by the thermal properties of the two plates through $\tau_1\tau_2=C_1$ and $\tau_1+\tau_2=C_2$. This explains the double time constant phenomenons of thermal pyranometers.

Inserting a sinusoidal change in radiation $G(t)=K\ \sin(\omega t)$ into Equation (2.17) yields:

$$K(1+(C_0\omega)^2)^{1/2}\ \sin(\omega t+\phi)=C_1\ \ddot{G}_1(t)+C_2\ \dot{G}_1(t)+G_1(t) \qquad (2.19)$$

where ϕ = arctan $(C_0\omega)$. The instrument response, determined by solving (2.19) analytically, is:

$$G_1(t)=A\ \exp(-t/\tau_1)+B\ \exp(-t/\tau_2)+\alpha K\ \sin(\omega t-\theta) \qquad (2.20)$$

where A and B are constants set by the initial conditions, τ_1 and τ_2 are the time constants of the two exponential components that appeared in the step response.

Once the elapsed time t exceeds τ_1 and τ_2 so that the transient terms approach zero, the signal $G_1(t)$ from the sensor lags behind the input radiation G(t) by the phase angle

$$\theta=\begin{cases}\arctan\ (\omega(\tau_1+\tau_2)/(1-\omega^2\tau_1\tau_2))-\phi & \text{if } \omega^2\tau_1\tau_2<1\\ \pi/2-\phi & \text{if } \omega^2\tau_1\tau_2=1\\ \pi+\arctan(\omega(\tau_1+\tau_2)/(1-\omega^2\tau_1\tau_2))-\phi & \text{if } \omega^2\tau_1\tau_2>1\end{cases} \qquad (2.21)$$

The signal from the sensor is also reduced in amplitude by a attenuation factor:

$$\alpha = \frac{[((1-\omega^2\tau_1\tau_2)^2+\omega^2(\tau_1+\tau_2)^2)(1+C_0^2\omega^2)]^{1/2}}{(\omega^2\tau_1^2+1)(\omega^2\tau_2^2+1)} \tag{2.22}$$

Both step and sinusoidal response of the double plate model are quite different from that of the single plate model.

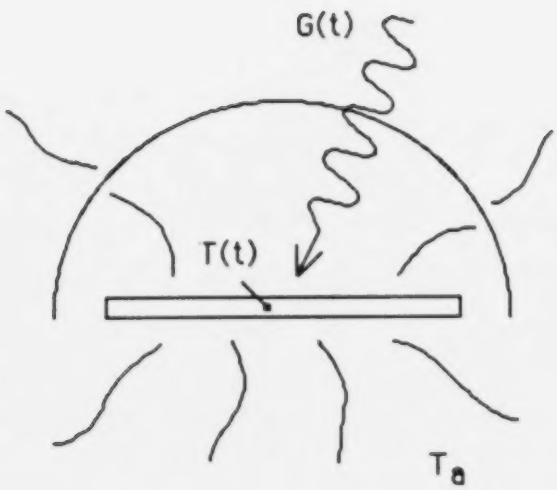

Figure 2.1 Single plate thermal pyranometer model.

Adapted from Suehrcke *et al.* [6].

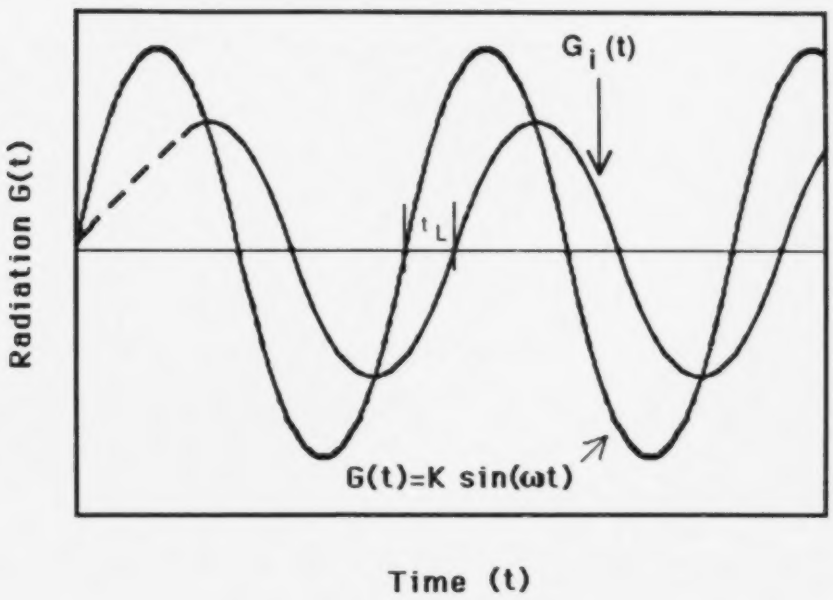

Figure 2.2 Sinusoidal response of single plate model.

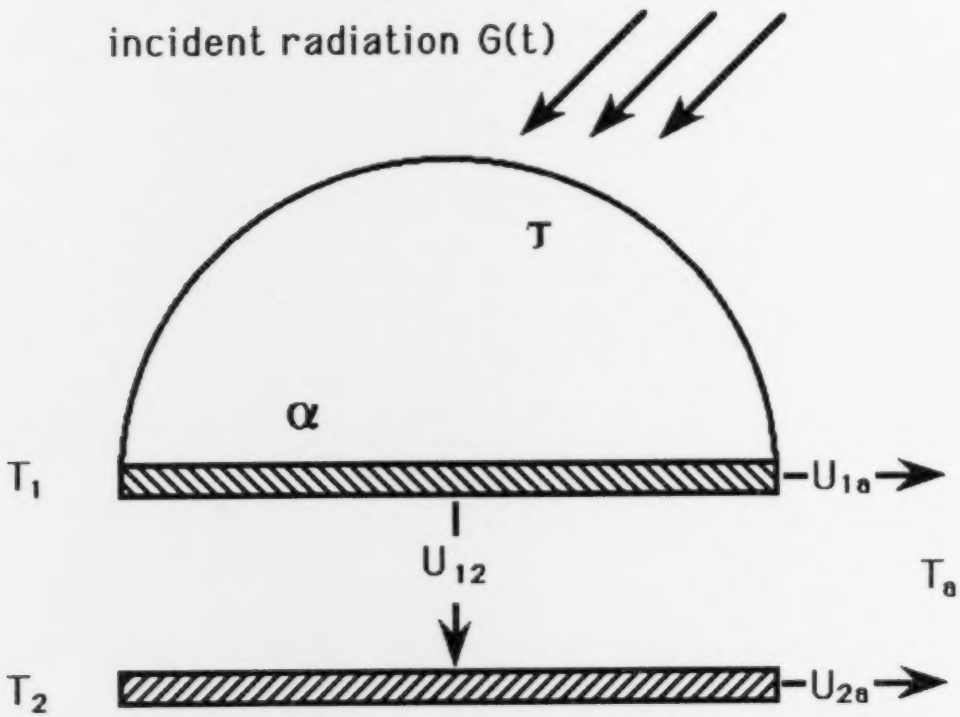

Figure 2.3 Double plate thermal pyranometer model.

3. STEP RESPONSE OF KIPP & ZONEN CM-5 PYRANOMETERS

The theoretical step response needs to be experimentally justified and the two time response constants determined for further investigation and correction of time response error. An experimentally-generated step change of radiation is used to examine the double time response phenomenon of Kipp & Zonen CM-5 pyranometers. Analysis of the signals produced by the pyranometers are to be used to show that the response to a step function can be described by the sum of two exponential components.

3.1 Instrumentation

The experimental setup is shown in Figure 3.1. A 600W tungsten filament projection lamp, operating under ac conditions, was used as the radiation source, and a step radiation change effected by the camera shutter. The step transition time was less than 1 ms. The intensity of the lamp was controlled by an ac autotransformer.

The radiation readings were recorded with a Sciemetric 8082A data acquisition unit and an IBM XT-compatible computer. The integrated data acquisition software COPILOT™ was used to monitor and store the signals.

3.2 Experimental results and analysis

The output signals were recorded once each second after the radiation step. Figure 3.2 shows a semi-logarithmic plot of one of measured responses to a downward step radiation change. For this plot, G_0= 780Wm^{-2} and G_1= 5Wm^{-2}. It is not possible to fit the points to a straight line, which is implied by Equation (2.5). But Equation (2.18), on the other hand, describes the observed experimental response.

But direct fitting of the recorded signal with (2.18) is susceptible to significant error in τ_1 and τ_2, as described by Acton [12]. Therefore general fitting schemes will not be used. To extract the two time constants τ_1 and τ_2, consider Equation (2.18), and assume that $\tau_1<\tau_2$. The first term on the right hand side of (2.18), with the time constant τ_1 and called the first signal component, decays faster than the second signal component with the time constant τ_2; it becomes negligible after a certain time. Figure 3.2 indicates the points closely fit a straight line after 20s, implying single exponential behavior there. Consequently the second signal is assumed to be dominant between 20 s and 60 s and readily determined by means of linear least squares fitting. As shown in Figure 3.2, the signal after 60 s cannot be accurately resolved by the data acquisition unit and is not considered in the analysis. The second signal component may now be subtracted from the original signal at times less than 15 s to obtain the first signal component. Figure 3.3 demonstrates this technique; the squares represent the extracted first signal component on the ln

$(G_1(t)-G_1)$ vs time diagram. The distribution falls on a straight line, verifying the two-exponential model for the thermal pyranometers.

From ten separate measurements of CM-5 pyranometer No. 784354, the average time constants were: τ_1=1.98±0.17 s and τ_2=11.79±0.24 s. The uncertainties represent the standard deviation of the ten measurements. All six of the pyranometers displayed a two-exponential response. Their values of τ_1 and τ_2, based on ten measurements for each pyranometer, are shown in Table 3.1.

Measurements of the time constants were performed under a variety of radiation inputs, varying parameters such as step amplitudes, step direction (upward or downward) and initial radiation (G_0). Good repeatability occurred for the two measured time constants. Step response experiments were also carried out under different physical conditions: different optical beam size centering on the sensor surface; illumination by the sun rather than a lamp; and different pyranometer orientations. The measured response times were not influenced by these conditions within the precision of our measurements.

The value of τ_1 agrees with the value of 3 s measured by van Wely and van den Brink [2] for a Kipp and Zonen CM-5 pyranometer. This reference makes no quantitative mention of τ_2, nor does τ_2 appear to have been measured elsewhere. A time constant of 235 s for a CM-5 pyranometer is indicated by Nast [8], although it is not clear whether this value is for τ_2 or some longer time constant.

3.3 Response to impulse radiation

Another property of pyranometer step response suggested by the experiments is that the ratio of A to B, which are the parameters in Equation (2.18), is a constant independent of operating conditions. This characteristic will produce an interesting phenomenon as the sensor undergoes an impulse radiation change.

Figure 3.4 shows how a double exponential response pyranometer reacts to an impulse radiation input theoretically. The impulse function is described by $G(t)=0$ for $t<0$, $G(t)=G_1$ for $0\le t<T$ and $G(t)=0$ for $t\ge T$, where T is small compared with the time constants τ_1 and τ_2.

During $0\le t<T$, the instrument responds as to a upward step radiation change determined by (2.18):

$$G_1(t)=A(1-\exp(-t/\tau_1))+B(1-\exp(-t/\tau_2)) \qquad (3.1)$$

At t=T, the first signal component reaches $A(1-\exp(-T/\tau_1))=A'$, and the second signal reaches $B(1-\exp(-T/\tau_2))=B'$. Now with the downward step occurring at this point, both signal components start to decay, but with a signal component ratio A'/B' rather than A/B. For $T<<\tau_1$, τ_2, $A'/B'\cong (A/B)(\tau_2/\tau_1)$. From the previous measurements for the time constants, $\tau_2/\tau_1\cong 5$, which is large enough to bring a significant change to the signal component ratio from A/B, which is what would be anticipated for a downward step.

In order to experimentally confirm the analysis, a function representing the signal component ratio at $t=t_0$, and independent of the absolute amplitude value of step or impulse is introduced. Slightly changing (2.18) for $t_0= 0$ yields:

$$G_1(t)- G_1= B\ (\mathcal{R}\ \exp(-t/\tau_1)+ \exp(-t/\tau_2)) \tag{3.2}$$

where $\mathcal{R}$ is the signal ratio at $t=t_0=0$.

Taking the logarithm and the derivative of (3.2) obtains:

$$\frac{d[\ln(G_1(t)-G_1)]}{dt} = \frac{d[\ln\ (\mathcal{R}\ \exp(-t/\tau_1)+ \exp(-t/\tau_2))]}{dt} \tag{3.3}$$

where the right hand side contains no absolute values, but only the ratio ($\mathcal{R}$) of A and B. Function (3.3) is used to characterize response with different $\mathcal{R}$.

In the experiment, the impulse radiation was generated by the camera shutter with T=0.25 s. CM-5 pyranometer #784354, with τ_1= 1.98 s and τ_2=11.79 s, was subject to the radiation input. The signal after the shutter closed was recorded every 0.3 second. To calculate function (3.3), each experimental data was first transformed to the logarithm of the difference between itself and the last stable signal. A series

of 20 transformed data points were then picked sequentially and regressed to a straight line by applying least squares fitting. Assigning the negative inverse of the slope of the regressed line, which is the response time in Suehrcke's model, to the times of the series middle points, a [-1/slope] vs time diagram like Figure 3.5 was obtained. In the diagram, the [-1/slope] at t=3 s is calculated by regressing the data points between 0.3 second and 6 second, and the [-1/slope] of 3.3 second by the data points between 0.6 and 6.3 second, and so on. The [-1/slope] vs time diagram of a downward step response is also displayed in the figure. Comparison with the theoretical calculation indicated that the impulse response fitted well with $\mathcal{R}$=40 curve and the step response with $\mathcal{R}$=7 curve. The impulse response has amplified value of $\mathcal{R}$ for the step response by about 6 times, confirming the previous analysis and the measured values of τ_1 and τ_2.

Impulse radiation response measurement also allow a simple way to estimate the first time constant τ_1 since the amplifying effect has made the first signal component take a major part right after the impulse. In Figure 3.5, the [-1/slope] of first few points of the impulse response approximately equals to τ_1.

3.4 Correction for measurement of step radiation

The experiments and analysis described above indicate that Kipp & Zonen CM-5 thermal pyranometers can be characterized by at least two exponential response times, which are independent of the measuring

range or physical conditions. From the measured values of τ_1 and τ_2, the parameters in (2.17) were readily obtained except the constant C_0. For a step radiation measurement, however, the term containing C_0 is zero because $\dot{G}(t)=0$ for $t \neq t_0$. A correction scheme is therefore possible using (2.17) to calculate G(t) from measured values of $G_1(t)$. A similar correction scheme has been proposed by Suehrcke *et. al.* [6] for a single exponential response pyranometer. The application of the two correction schemes to a downward step function is shown in Figure 3.6, which compares the pyranometer signals $G_1(t)$ with the corrected readings. With Suehrcke's first order correction method [6], τ_1 is used as the time constant. For this figure, t_0=1s, G_0=780Wm^{-2}, G_1=5Wm^{-2}.

The corrected readings are a definite improvement over the CM-5 pyranometer readings, effectively approaching the true radiation G_1 about 10 s after the step. The first order correction scheme also shows improvement over the uncorrected signal, but the decay to the true signal is slower than with the second order method. This is due to the uncorrected second exponential component.

Thus the time response error of a step response has been successfully compensated using the measured time constants which determine C_1 and C_2 in Equation (2.17). But a realistic radiation variation is more arbitrary and the C_0 term in (2.17) needs to be considered if we wish to apply the second order correction method for a more general instantaneous solar radiation measurement. Like the other constant factors in (2.17), C_0 is determined by the thermal properties of the

radiation sensor. A theoretical calculation of C_0 is virtually impossible because of the difficulty obtaining the sensor thermal parameters. As has been discussed above, the sinusoidal response of the thermal pyranometer model, either through the attenuation factor α or phase lag θ, is influenced by C_0, since a sinusoidal variation of G(t), unlike a step function, does not set the term containing C_0 in (2.17) to zero. Therefore a sinusoidal response experiment is needed in order to correct the second order response error caused by an arbitrary radiation signal. This experiment is discussed in the next chapter.

Serial #	$\overline{\tau_1}$ (s)	$\Delta\tau_1$ (s)	$\overline{\tau_2}$ (s)	$\Delta\tau_2$ (s)
784332	2.87	0.027	11.95	0.15
784316	2.83	0.037	9.92	0.12
784396	2.32	0.059	10.78	0.14
784386	2.91	0.035	13.43	0.07
784354	1.98	0.170	11.79	0.24
784356	2.55	0.180	10.62	0.21

Table 3.1 The value of τ's of six pyranometers.

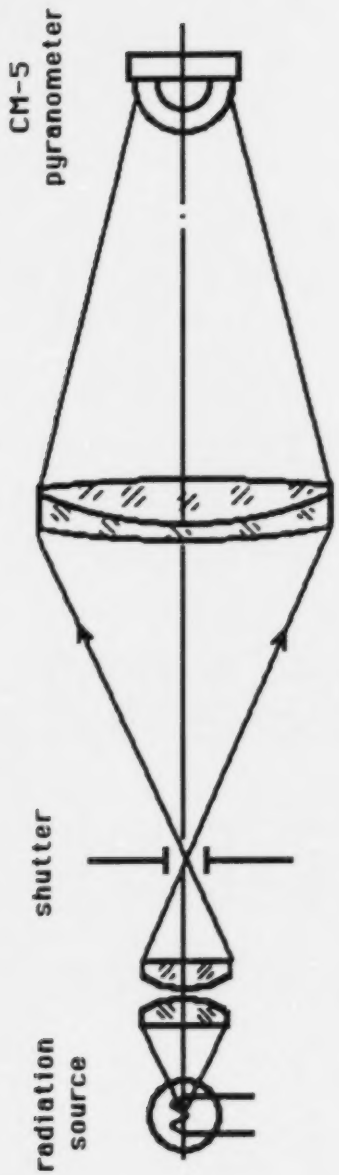

Figure 3.1 Experimental setup for step response measurement.

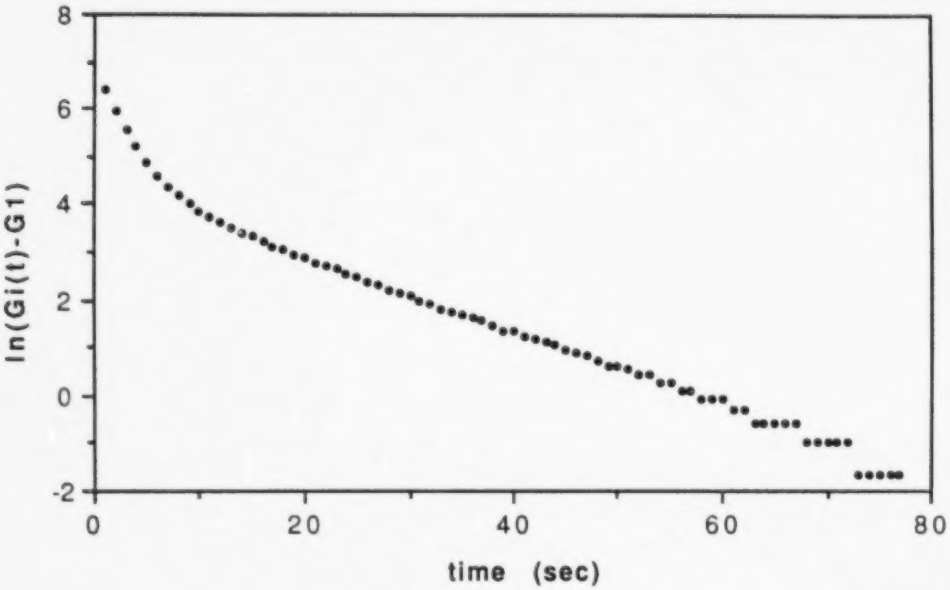

Figure 3.2 Pyranometer response to a downward step of radiation.

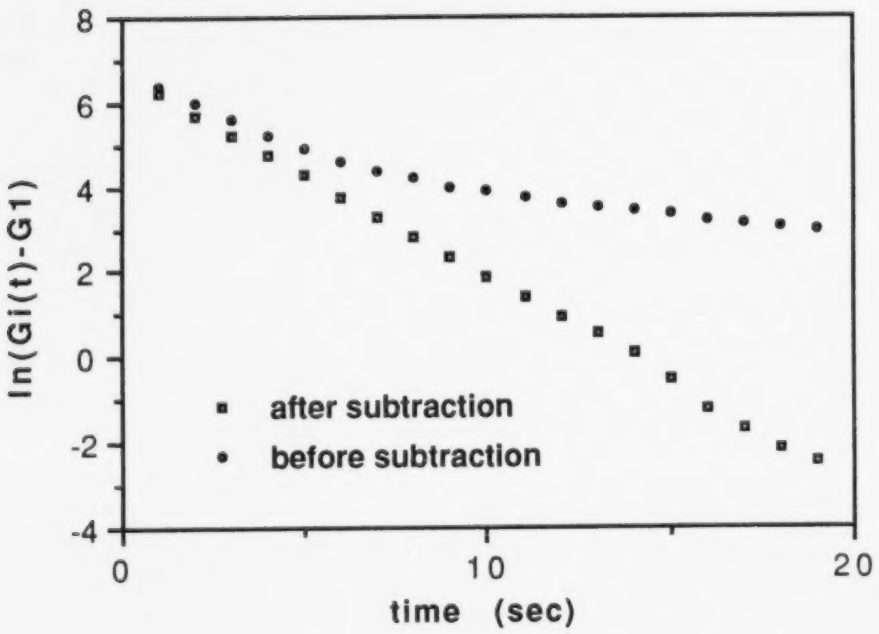

Figure 3.3 Extraction of τ_1 signal from the original signal.

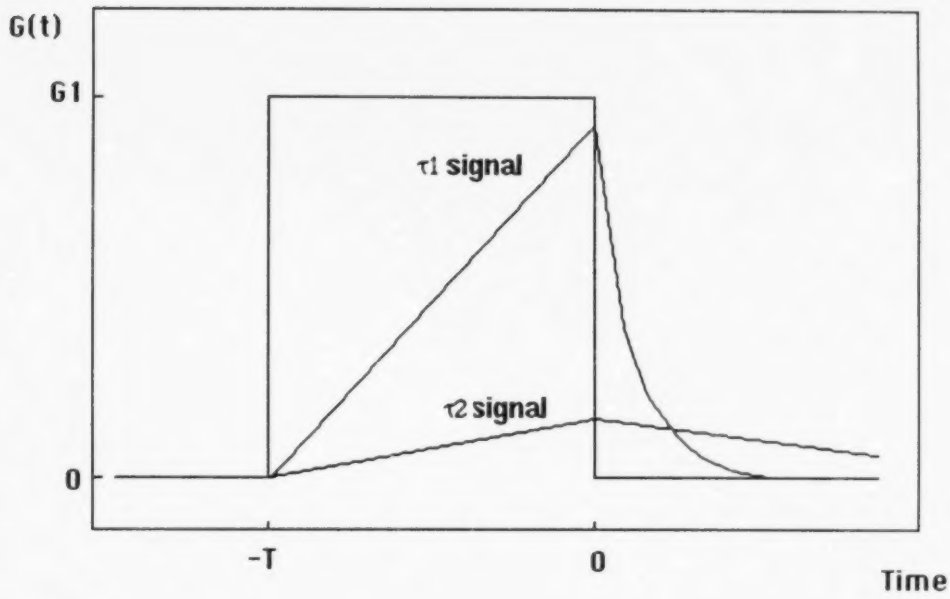

Figure 3.4 Pyranometer response to a pulse radiation.

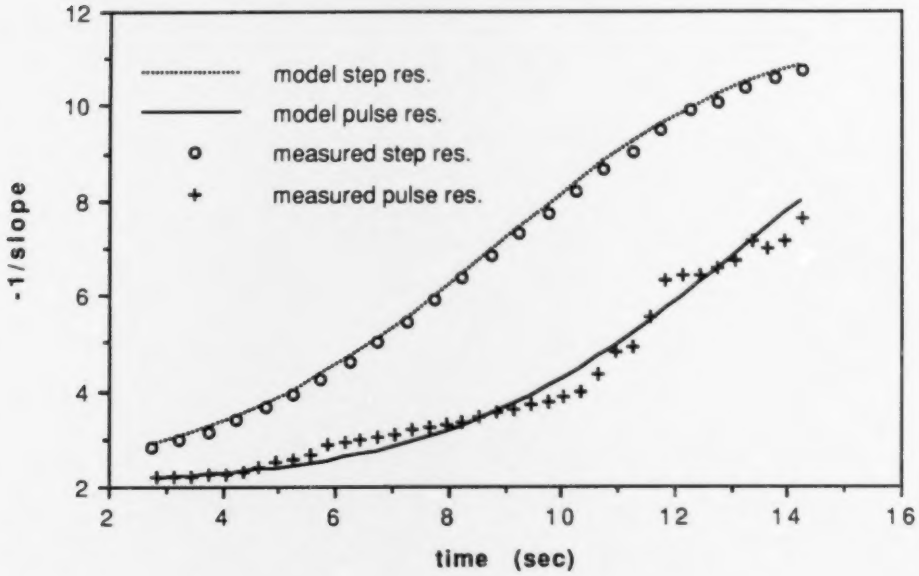

Figure 3.5 Comparison between the pulse and the step response.

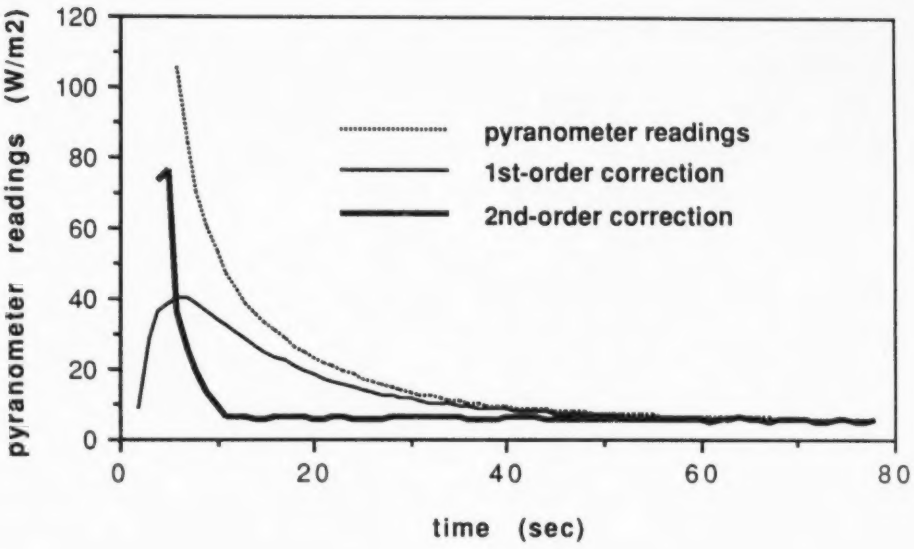

Figure 3.6 First and second order corrections to the pyranometer readings for a downward step of radiation.

4. SINUSOIDAL RESPONSE OF KIPP & ZONEN CM-5 PYRANOMETER

In the previous chapter, the investigation of the step radiation response of Kipp & Zonen CM-5 pyranometers shows that the response to a step function should be described by the sum of two exponential functions [13, 14]. A two plate thermal model was developed and the relationship between the radiation input G(t) and the pyranometer output $G_1(t)$ satisfied the differential equation (2.17), in which the constant factors C_1 and C_2 are readily known once the two time constants τ_1 and τ_2 are measured. For step radiation input, the time response error has been compensated by using (2.17) directly [13, 14]. To correct the time response error for an arbitrary input G(t) however, another constant C_0 in (2.17) must be determined.

From (2.21) and (2.22), sinusoidal response of the two plate sensor model depends on not only the two time constants but the constant C_0 as well. With known τ_1 and τ_2, C_0 can be obtained by measuring the sinusoidal response of the pyranometer.

4.1 Experimental setup

Figure 4.1 shows the experimental setup. A 600W tungsten filament projection lamp was used as the radiation source. Kipp & Zonen CM-5 thermal pyranometer #784316 and a Rho Sigma photovoltaic pyranometer were used for the sinusoidal response measurement. The beam splitter

permits simultaneous thermal and photovoltaic sensor measurements. Because of its rapid response, the photovoltaic sensor is assumed to give readings proportional to the incident radiation,* with no error due to a finite response time.

The sinusoidal modulator is an opaque template of radius $\rho=R+r \sin \gamma$, as shown in Figure 4.2. Assuming the lamp filament has a rectangular image of uniform intensity, the radiation transmitted past the modulator is proportional to the dashed area. If the template rotates at a constant rate, the radiation reaching the sensor will be sinusoidally modulated. To vary the angular frequency ω for the sinusoidal function generator, the template was driven by a small rubber wheel, whose distance from the template axis could be changed by physically moving the wheel. The rubber wheel was driven by a synchronous motor with speed of about 6 rpm.

The radiation readings were recorded with a Strawberry Tree Analog Connection™ Mini-16™ data acquisition unit and an IBM-XT compatible computer. The QuickLog PC™ software was used to monitor and store signals.

4.2 Measurement and analysis

The data acquisition procedure started after the thermal pyranometer

---

* Due to the principle of operation of the sinusoidal modulator, the uneven temperature distribution on the lamp filament image may change the spectral content of the modulated light beam. The possible error caused by the spectral sensitivity of the PV sensor is ignored here.

reached its stable status, i.e. the transient terms in (2.20) became zero. The output signals from the pyranometers were sampled and stored once each 0.5 s in a data file. Figure 4.3 displays the sampled data at ω=0.4009 rad s^{-1}. Some ripple appears on the photovoltaic pyranometer output. This is caused by the ac power supply powering the light source. The thermal pyranometer output is still not a pure sinusoidal function although less ripple is present than on the photovoltaic signal. That is probably due to limitations in the sinusoidal modulator. For instance, the imperfection of the modulator template shape and the lamp filament image would influence the purity and spectral pattern of the generated sinusoidal function.

Before performing the numerical calculation of lag time or attenuation factor indicated by (2.21) and (2.22), an accurate frequency determination was necessary. That is because the angular frequency ω of each data file is only roughly estimated at this point and its 'true' value has to be determined by the signals themselves.

A program, shown in Figure 4.4, was written for the purpose of determining the frequency. Because of its smaller ripple, the thermal pyranometer signal was used. Only an initially estimated frequency ω and the changing step $\Delta\omega$ are needed as input parameters to the program. Δi, assumed to have only one minimum value with different ω, are the standard deviation of the experimental data and their best fitting sinusoidal function. Comparison of Δi's of different ω determine the direction of adjusting ω. The best fitting angular frequency (ω) is yielded automatically with the accuracy of $\pm\Delta\omega$. The

results shown in the thesis were obtained by $\Delta\omega$=0.0001 rad/s. The source file of the program is given in Appendix A.

Using the calculated ω to fit the experimental data, the lag time and the amplitude attenuation of the thermal pyranometer output were determined. The amplitude attenuation measurement suffers from a basic inaccuracy caused by difficulties experienced in initially equalizing the signals from the two pyranometers at their minimum and maximum values at the two corresponding positions of the modulator template. This may be caused by non-linear effects of the modulation process, or variation of the optical frequency components of the radiation emitted from different portions of the lamp filament. Fortunately, the lag time measurement accuracy does not depend on the signal equalization accuracy of the sensors. Thus only the lag time measurement was used to determine the unknown constant C_0 in (2.17).

The sinusoidal response of the Kipp and Zonen CM-5 pyranometer #784316 has been measured under 14 different frequencies ranging from 0.0891 to 0.4617 rad s^{-1}. For this pyranometer, τ_1 and τ_2 were measured to be 2.83 s and 9.97 s, respectively (See Table 3.1). The lag time vs. angular frequency diagram is plotted in Figure 4.5.

The theoretical curve displayed in Figure 4.5 is plotted according to (2.21) for C_0=9.22±0.02 s. This value of C_0 was obtained from a fit of (2.21) to the experimental points for a chi-squared minimum. The quoted uncertainty is the value of $\sqrt{\chi^2}$.

For completeness, the attenuation diagram is displayed in Figure 4.6. The experimental and calculated results show reasonable agreement, although the theoretical curve for C_0=9.22 consistently falls below the experimental points. Presumably, this is due to the inaccuracy of the attenuation measurement.

4.3 Conclusions

The sinusoidal response of Kipp and Zonen CM-5 pyranometer with angular frequency ω has been measured over the frequency range 0.014-0.073 Hz. Comparing the experimental data with theoretical calculations based on the two plate thermal sensor model has determined the last unknown constant of (2.17) so that all the parameters appearing in the transient function have been experimentally obtained. On the other hand, the good agreement between the measured and calculated sinusoidal response has given a justification for the previous model analysis.

With the known transient function, representing the relationship between the pyranometer input and output, a correction scheme should be possible by computing the pyranometer input, which is the 'true' value of the incident radiation, from the pyranometer output, that is, the radiation value indicated by the instrument.

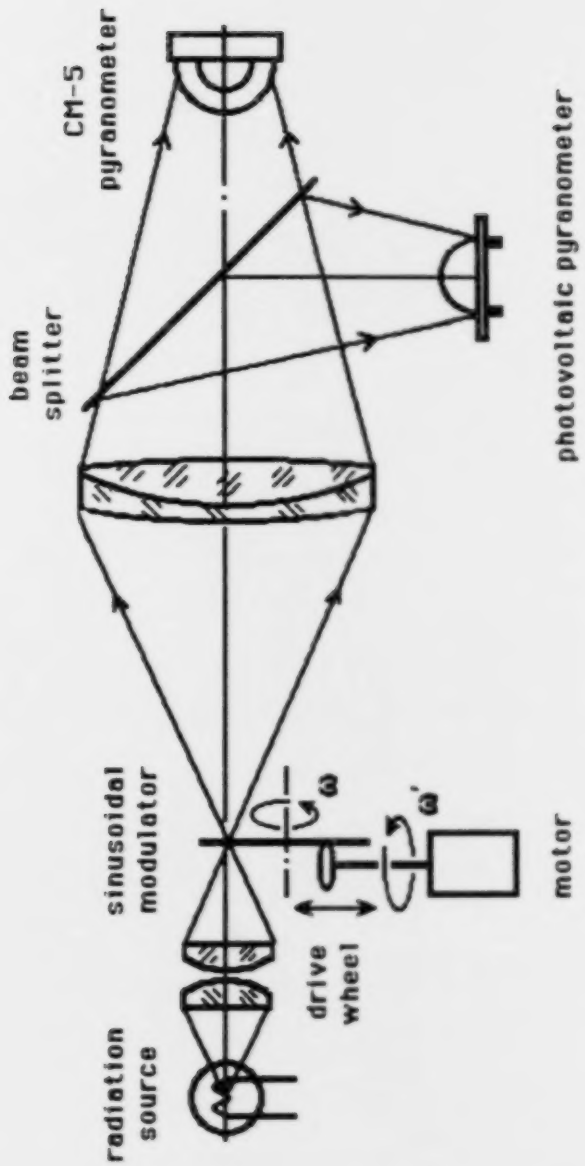

Figure 4.1 Experimental setup for the sinusoidal response measurements

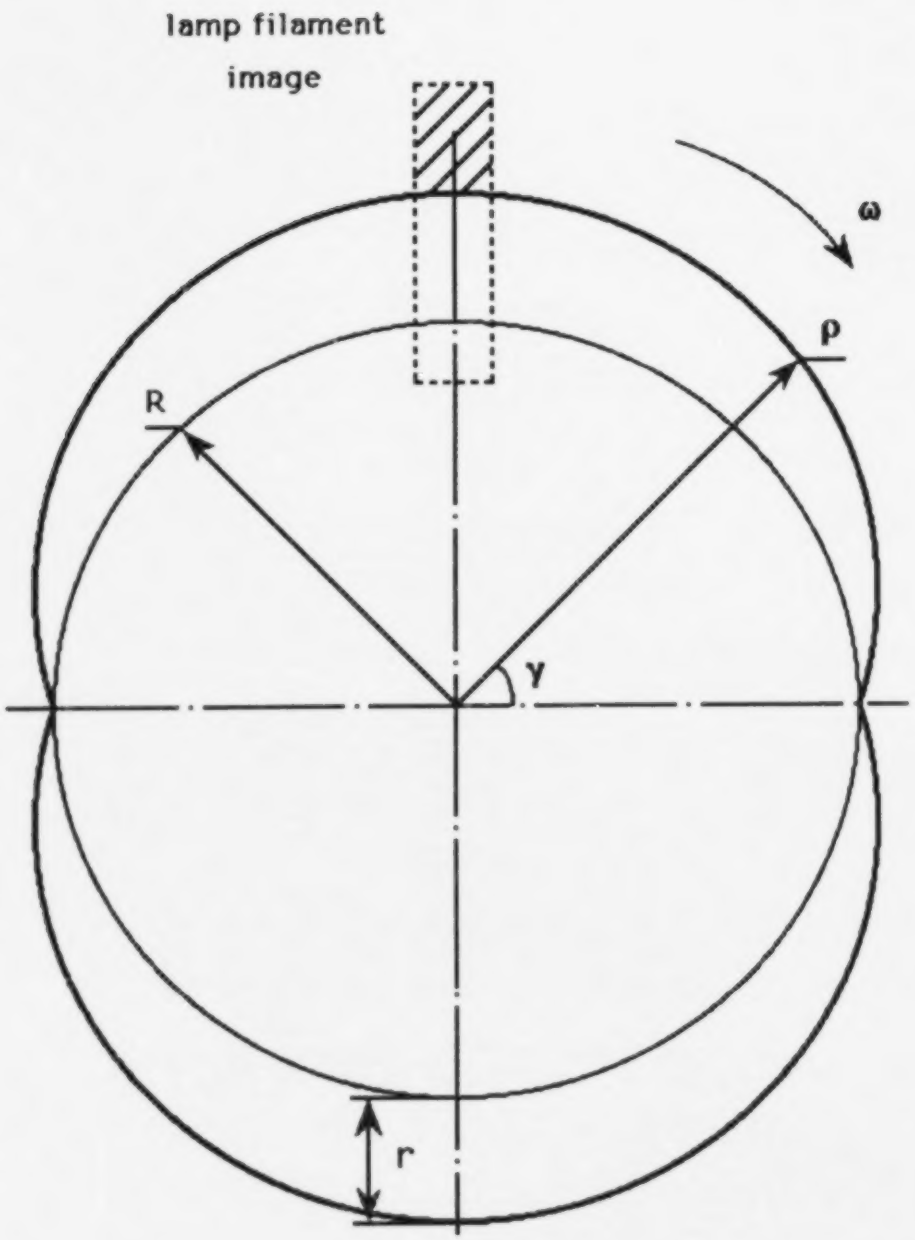

Figure 4.2 Shape of the sinusoidal modulator template.

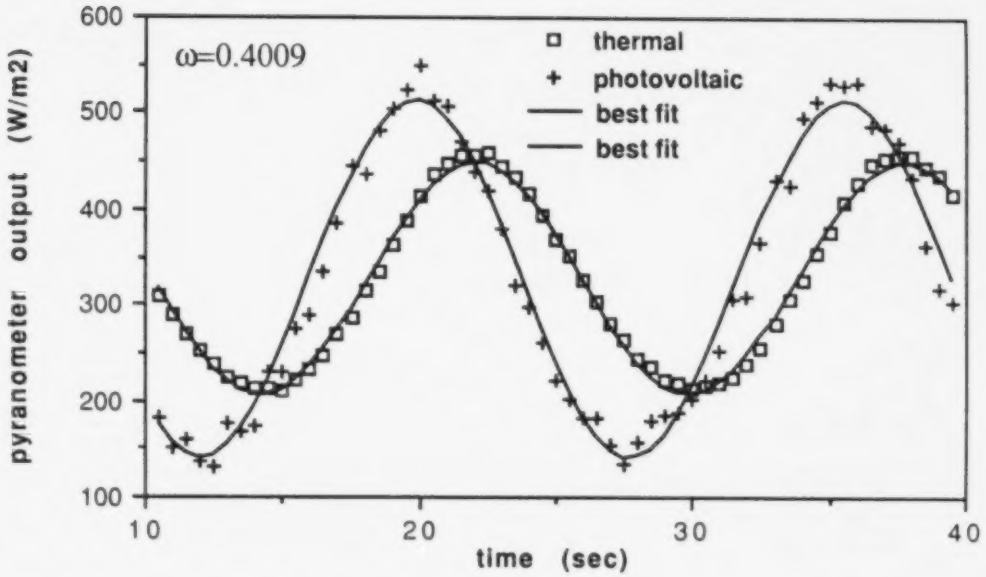

Figure 4.3 Sinusoidal response of the thermal and photovoltaic pyranometers.

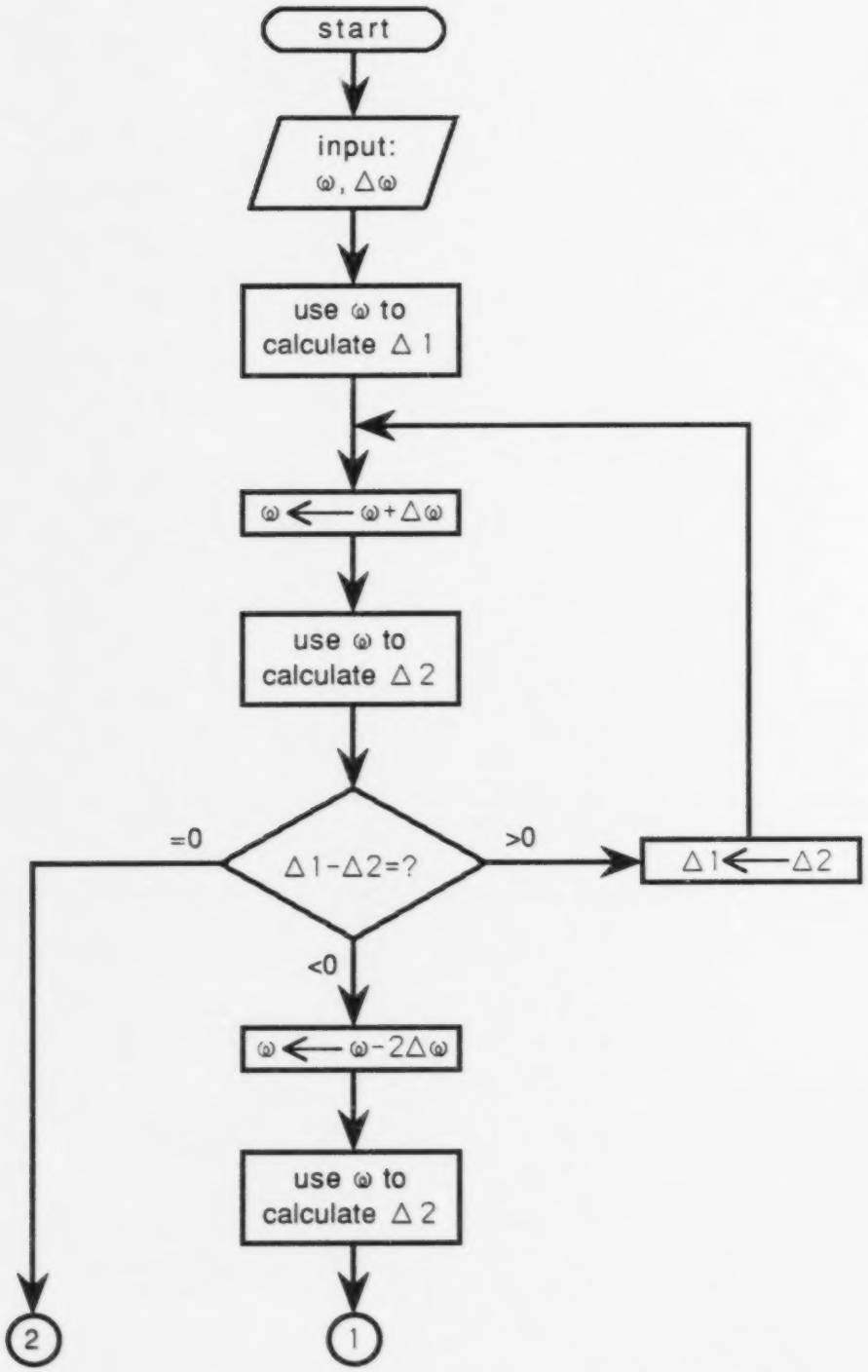

Figure 4.4 Flowchart of frequency (ω) optimization program

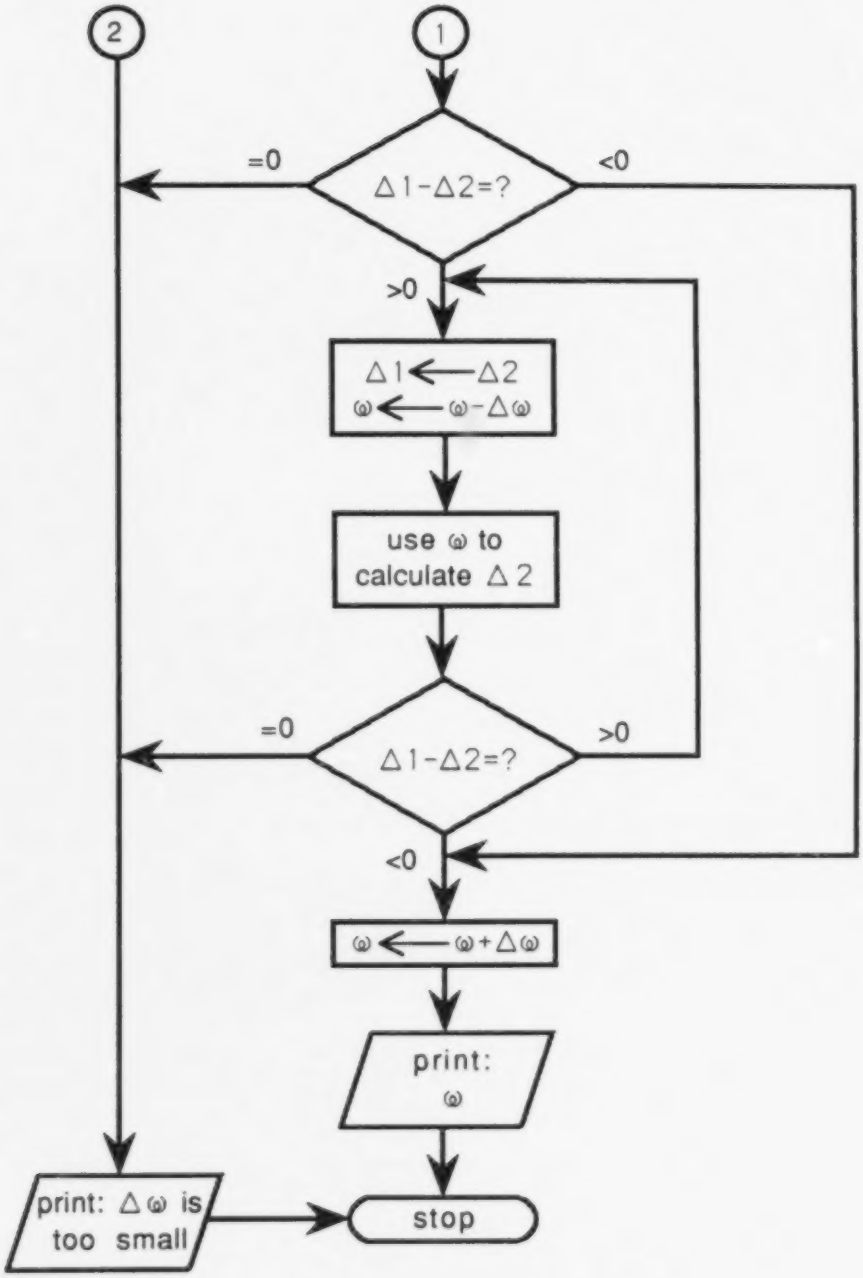

Figure 4.4 (Continued)

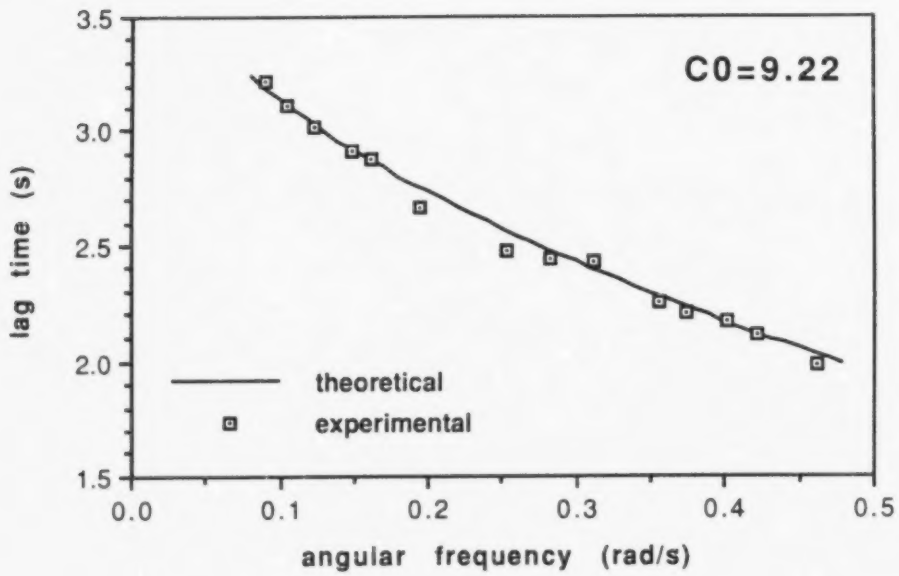

Figure 4.5 Lag time of sinusoidal response between the pyranometers.

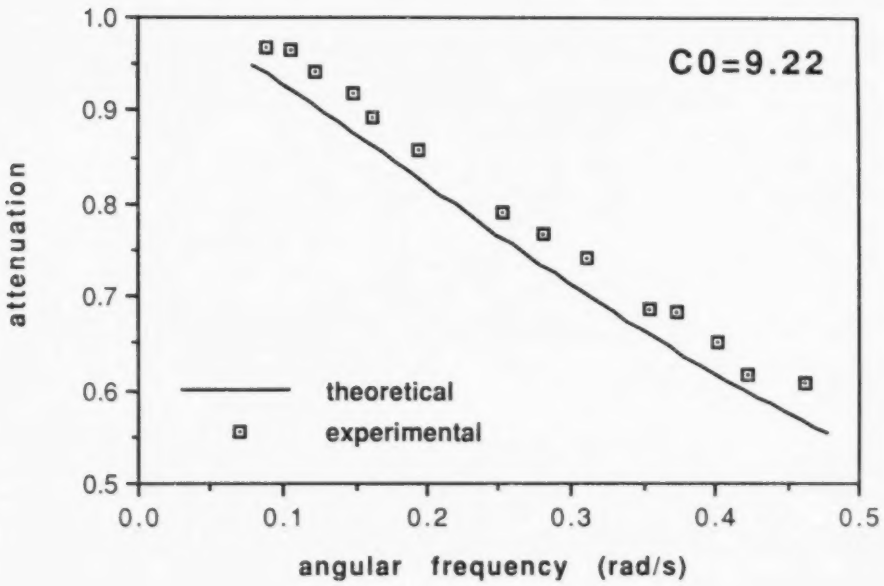

Figure 4.6 Attenuation of sinusoidal response of the thermal pyranometer.

5. TIME RESPONSE ERROR CORRECTION

5.1 Introduction

The measurements of the step response and the sinusoidal response of Kipp and Zonen CM-5 pyranometer have quantitatively explored the relationship between the pyranometer input and the output. At this point, the transient function (2.17) can be used to determine the radiance input G(t) according to the instrument output $G_i(t)$. But the calculation procedure from $G_i(t)$ to G(t) will involve not only the numerical solution for a differential equation, but also numerical differentiation for the values of the first and second derivatives of G_i. As numerical differentiation is always fraught with difficulties and hazards, it should be performed with caution.

5.2 Numerical differentiation

The derivative of the function $G_i(t)$ at $t=t_0$ is defined as

$$G_i(t)=\lim_{\Delta t\to 0}\frac{G_i(t_0+\Delta t)-G_i(t_0)}{\Delta t} \tag{5.1}$$

provided the limit exists. For a tabulated set of experimental data, the way in which $G_i(t)$ usually appears, the accuracy of numerical

differentiation depends largely on the measurement accuracy and the sampling frequency. Since measurement error exists, however, decreasing Δt (increasing the sampling frequency) will not guarantee a better result of differentiation. In some cases smaller Δt amplifies the error of differentiation with the existence of measurement error. Figure 5.1 demonstrates the phenomenon. The slope of L, measured with larger sampling period Δt, approximates the true derivative (the slope of the tangent) rather than the slope of L', which is measured with smaller sampling period $\Delta t'$, even when the same amount of error e is introduced in both measurements. In addition, the error in the first derivative will be transferred to the calculation of the second derivative and make the situation worse.

5.2.1 3-point collocation

The simplest and most straightforward algorithm for the numerical computation of first and second derivatives is the three point collocation method by calculating $\dot{G}_i(t)$ using $G_i(t-\Delta t)$ and $G_i(t+\Delta t)$, where Δt is the sampling period. $\dot{G}_i(t)$ is approximated by the slope of the line passing through its two neighboring points:

$$\dot{G}_i(t) = \frac{G_i(t+\Delta t) - G_i(t-\Delta t)}{2\,\Delta t} \qquad (5.2)$$

Replacing G_i with $\dot{G}_i$ will obtain the second order derivative as well.

As discussed before, a step radiation input will set the differential term in (2.17), $C_0\dot{G}(t)$, to zero. As a consequence, how well the time response error is compensated depends on how accurately the values of $\dot{G}_i$ and $\ddot{G}_i$ are calculated. Thus the result of error correction for step response can be used as an indication for the derivative calculation. In another words, the compensation for the step response can be used to determine which numerical differentiation scheme should be used.

Figure 5.2 displays the corrected step response using 3-point collocation numerical computation. Substantial ripple appears on the corrected curve. The situation is even worse right after onset of the step because the steeper response curve there makes the derivative calculations less accurate.

A 3-point collocation algorithm is not suitable for the correction scheme because it directly utilizes the result of the experiments, completed with inherent measurement errors. Moreover, these inherent errors usually will not be predictable with any degree of certainty; that is to say, the inherent errors are distributed according to some statistical pattern, and there is a reasonable probability that some of the errors are quite large. Thus a smoothing procedure for the experimental data is preferable before performing derivative calculations.

5.2.2 Data smoothing

Least squares approximations are often used as a effective scheme to

smooth out inherent errors. However the signals from the pyranometer can change in an arbitrary fashion caused by the cloud passing between the sun and the pyranometer. It is impossible, therefore, to fit the radiation readings with any particular simple function. However, it is reasonable to assume that the radiation change in a small period of time, say 2 or 3 seconds, shouldn't be very large and could be fitted by a simple function. In the case of the sample period being 0.5 s, it should be reasonable to assume that 5 successive points - representing a period of 2 seconds - can be well fitted by a quadratic curve. Thus a 5-point parabola fitting algorithm is used in the numerical differentiation for the purpose of smoothing data. By this method, $\dot{G}_i(t)$ is calculated by using five successive values of G_i straddling the reading at t. The numerical differentiation formula for 5 point parabola fitting has been given by LaFara [15]:

$$\dot{G}_i(t) = \frac{1}{10\ \Delta t}\left(-2\ G_i(t-2\ \Delta t) - G_i(t-\Delta t) + G_i(t+\Delta t) + 2\ G_i(t+2\ \Delta t)\right) \quad (5.3)$$

where Δt is the sampling period. $\ddot{G}_i$, in turn, is obtained from the five successive values of $\dot{G}_i$ straddling the point at t.*

Because (5.3) does not apply near both ends of the data, the following

---

* With a 5-point parabola fitting scheme, $\ddot{G}_i$ could also be calculated directly from the fitted cuve of G_i, in which case less points will be used to calculate the second derivative. But that will eventually increase the truncation error as stated by Dorn [16].

formulas obtained from four point parabola fitting will be useful for the points at each end [15]:

$$\dot{G}_i(t_0) = \frac{1}{20\,\Delta t}\,(-21\,G_i(t_0)+13\,G_i(t_0+\Delta t)+17\,G_i(t_0+2\,\Delta t) -9\,G_i(t_0+3\,\Delta t)) \tag{5.4}$$

$$\dot{G}_i(t_0+\Delta t) = \frac{1}{20\,\Delta t}\,(-11\,G_i(t_0)+3\,G_i(t_0+\Delta t)+7\,G_i(t_0+2\,\Delta t) G_i(t_0+3\,\Delta t)) \tag{5.5}$$

$$\dot{G}_i(t_N-\Delta t) = \frac{1}{20\,\Delta t}\,(11\,G_i(t_N)-3\,G_i(t_N-\Delta t)-7\,G_i(t_N-2\,\Delta t) - G_i(t_N-3\,\Delta t)) \tag{5.6}$$

$$\dot{G}_i(t_N) = \frac{1}{20\,\Delta t}\,(21\,G_i(t_N)-13\,G_i(t_N-\Delta t)-17\,G_i(t_N-2\,\Delta t) +9\,G_i(t_N-3\,\Delta t)) \tag{5.7}$$

where the last data point is at t_N.

Figure 3.6 shows the consequence of using 5-point-parabola fitting. Compared with Figure 5.2, the noise produced by the differentiation calculation is greatly reduced at the price of the corrected readings approaching G_1 after 10 s of step onset, much slower than the 3 point collocation scheme. That is because more points were used in the

derivative computation and the under-approximation for the values of first few point derivatives made the error compensation there insufficient. It has to be pointed out that the experimentally generated step radiation change, with a rise time of less than 1 ms, is much more rapid than what can occur in actual solar radiation measurement. The accuracy of the derivative calculation using 5 point parabola fitting will improve when the input radiation doesn't change so rapidly.

5.3 Time response error correction

5.3.1 Runge-Kutta method

For an arbitrary radiation input G(t), calculating G(t) from $G_i(t)$ with (2.17) is a problem of solving a first-order ordinary differential equation. Many numerical techniques exist for finding the solutions to differential equations. Because of the difficulties encountered in numerical differentiation as discussed before, the fourth-order Runge-Kutta method is used because it does not require the evaluation of any derivatives. However, function $\dot{G}(t)$ will have to be evaluated for more than one value of t and G(t) [16], that is to say that two successive values of $G_i(t)$ will be used to evaluate one value of G(t) and the consequent data points will have only half the number of $G_i(t)$ values. But this disadvantage will be well compensated by not having to evaluate the derivatives.

According to (2.17), the fourth-order Runge-Kutta in this problem can

be defined by the following five equations:

$$G(t+2\ \Delta t)= G(t)+ \Delta t(k_1+2k_2+2k_3+k_4)/3 \tag{5.8}$$

where Δt is the sampling period and

$$k_1=(C_1\ddot{G}_i(t)+C_2\dot{G}_i(t)+G_i(t)-G(t))/C_0 \tag{5.9}$$

$$k_2=(C_1\ddot{G}_i(t+\Delta t)+C_2\dot{G}_i(t+\Delta t)+G_i(t+\Delta t)-G(t+\Delta t)-\Delta t\ k_1))/C_0 \tag{5.10}$$

$$k_3=(C_1\ddot{G}_i(t+\Delta t)+C_2\dot{G}_i(t+\Delta t)+G_i(t+\Delta t)-G(t+\Delta t)-\Delta t\ k_2))/C_0 \tag{5.11}$$

$$k_4=(C_1\ddot{G}_i(t+2\ \Delta t)+C_2\dot{G}_i(t+2\ \Delta t)+G_i(t+2\ \Delta t)-G(t+2\ \Delta t)-2\ \Delta t\ k_3))/C_0 \tag{5.12}$$

Provided the initial value $G(t_0)$ is known, the $G(t)$ after t_0 can be evaluated with the time period of $2\ \Delta t$.

5.3.2 Initial condition and partial instability

Because the time response error correction involves the numerical solution for a differential equation, it is important to know the initial value of the 'true' incident radiation $G(t_0)$. In addition to this, the partial instability may be encountered [16] when too many steps are taken in solving the equation and produce extremely inaccurate results, because small roundoff or truncation errors may be accumulated and magnified as the solution is carried out over a large

number of time steps.

According to the previous sensor model analysis, it is assumed that whenever the sensor plate temperature reaches equilibrium, the instrument will give a correct reading for the radiation, i.e. $G_i(t)=G(t)$, if $\ddot{G}_i(t)=\dot{G}_i(t)=0$. With this property, a procedure was invoked in the error correction program to refresh the initial input radiation value occasionally. The first and the second derivatives of $G_i(t)$ were monitored and when they were small enough, $G_i(t)$ would be assumed to represent the input radiation and used as the initial G(t) for the following data points.

In realistic solar radiation measurements, more than 80% of the time is occupied by clear sky or totally cloudy conditions ($\ddot{G}_i(t)=\dot{G}_i(t)=0$) [3], when there is no instrument response problem at all. Thus the initial value refreshing procedure not only prevents continuous propagation of numerical error inherent in the Runge-Kutta method, but also eliminates unnecessary calculation when the time response error doesn't occur. The Turbo Pascal program for the 2nd order time response error correction is given in Appendix B.

5.3.3 Error correction for experimentally generated radiation

The experimental setup for the sinusoidal response measurement (Figure 4.1) was used to demonstrate the utility of both first order and second order correction schemes. Without the sinusoidal modulator, the intensity of the projection lamp was varied by rotating in an

arbitrary fashion the control knob of the autotransformer powering the lamp. Figure 5.3 plots typical thermal and photovoltaic pyranometer signals subjected to the 'arbitrary' intensity, with the results of the second order correction (SOC) scheme applied to the thermal pyranometer readings. For comparison, the first order correction (FOC) of Suehrcke [6] was also applied. Figures 5.3 (a) and (b) are segments of the same intensity scan, while Figure 5.3 (c) is from another scan. Note the different horizontal and vertical scales of Figure 5.3 (b) compared with the other two figures.

In general, the corrected readings closely follow the photovoltaic signal, which is assumed to be proportional to the incident radiation G(t). Under most circumstances, the SOC is a substantial improvement over the FOC although they are both nearly equal when G and G_1 are not rapidly changing, as, for example, for $t \leq 8$ s.

Both correction schemes do not respond to intensity spikes of width of approximately 1s or less. These spikes were intentionally produced by 'tweaking' the autotransformer dial, for example at $t \cong 19$, 34, 37, and 40 s. The 1 s duration represents probably the fastest that could be produced by cloud edges or 'holes' in clouds passing between the sun and the pyranometer. The thermal pyranometer does not react significantly to such spikes because of its longer time response. As well, the numerical technique for determining the first and the second derivatives at a given point uses a small spread of contiguous points, which tends to wash out any such short duration structure.

A good example illustrating the difference between the SOC and the FOC scheme is demonstrated at t≅41 s in Figure 5.3 (b). At this time, $\dot{G}_i=0$ and according to the FOC scheme [6], $G_i \cong G$, which is indeed the case, as evident in the figure. On the other hand, the SOC curve is not equal to G_i because $\ddot{G}_i \neq 0$ and it is much closer to the true curve G.

One property of the numerical technique used for correcting the signal is apparent at t=66 s in Figure 5.3 (c). G(t) decreases rapidly at this time, and both the FOC and SOC schemes seem to 'anticipate' this decrease before it actually occurs, by commencing to drop a little beforehand. This occurs because of the method of numerical differentiation to determine $\dot{G}_i$ and $\ddot{G}_i$. As has been discussed, $\dot{G}_i$ at t is calculated by using the five successive values of G_i straddling the reading at t. As well, $\ddot{G}_i$ is obtained from the five successive values of $\dot{G}_i$. Thus the calculation at t 'looks ahead' 4 Δt actually. One could perform the numerical differentiation using past times only to avoid this effect, but would possibly produce less accurate values of the derivatives elsewhere [18].

The SOC scheme results in a signal which very closely matches that of the incident radiation. Applying this scheme in 'real time' should be possible if required, where, because of the numerical differentiation technique discussed above, 'real time' actually means correcting the signal after a delay of approximately 4Δt. The computer used for controlling the data acquisition unit and for calculating the correction must be able to perform the correction in less than Δt.

Furthermore, the FOC developed above may generally be used for other sensors, such as the temperature sensors, of which the dynamic character can be described by a multi-exponential function.

5.3.4 Error correction for solar radiation measurement

In order to demonstrate the SOC application in the actual solar radiation measurements, one Kipp & Zonen CM-5 thermal pyranometer and one Rho Sigma photovoltaic pyranometer were installed horizontally on the roof of the Electrical Engineering Building in the University of Alberta. On August 20, 1991, a fast variation of cloud thickness was recorded around 1:30 pm by both the thermal and the photovoltaic pyranometer. The pyranometer readings are shown in Figure 5.4 as well as the compensated curves obtained by both correction schemes.

It is obvious that the SOC scheme is a definite improvement over not only the thermal pyranometer readings but also FOC scheme.

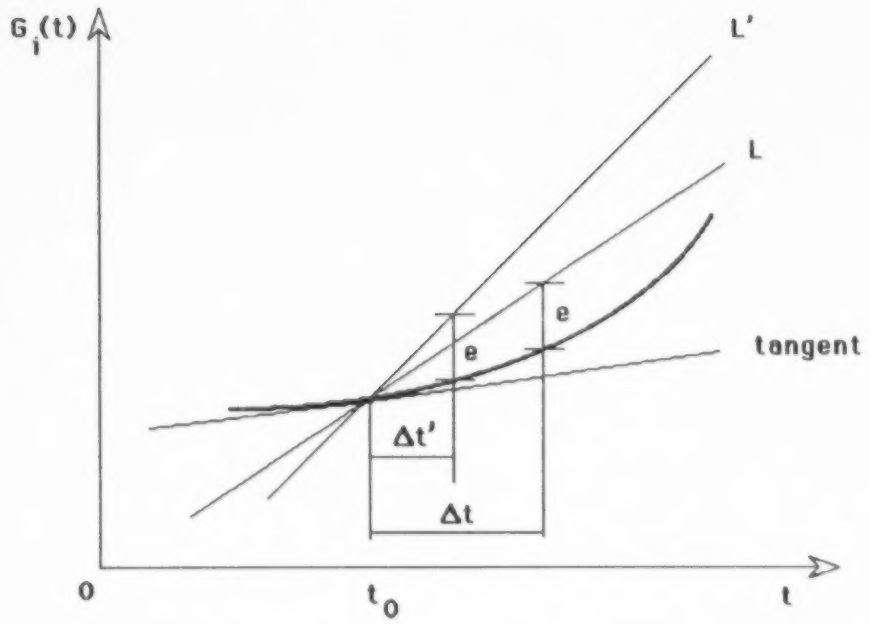

Figure 5.1 Demonstration of how smaller Δt can increase the differentiation error.

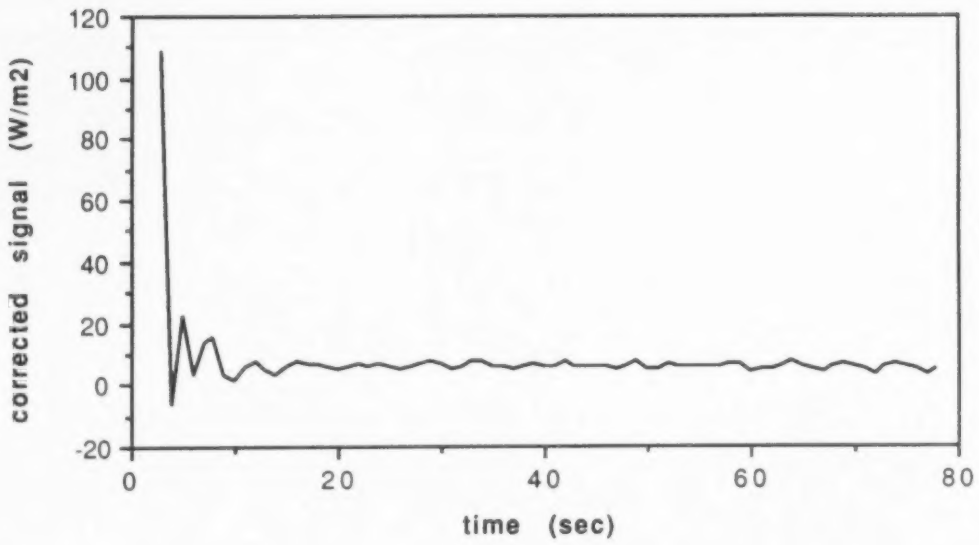

Figure 5.2 Step response correction using 3-point collocation method.

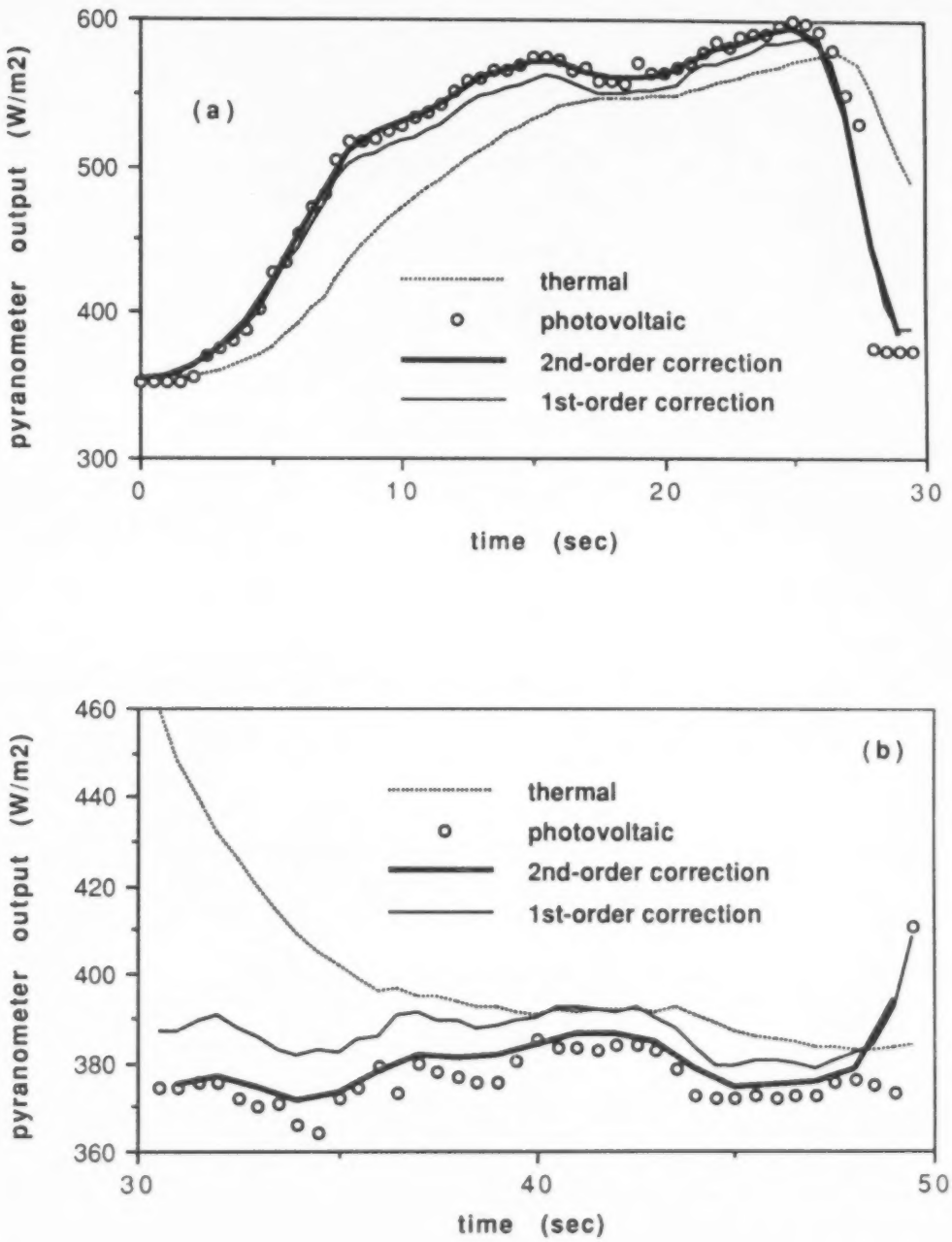

Figure 5.3 Response time FOC and SOC to an arbitrary radiation signal.

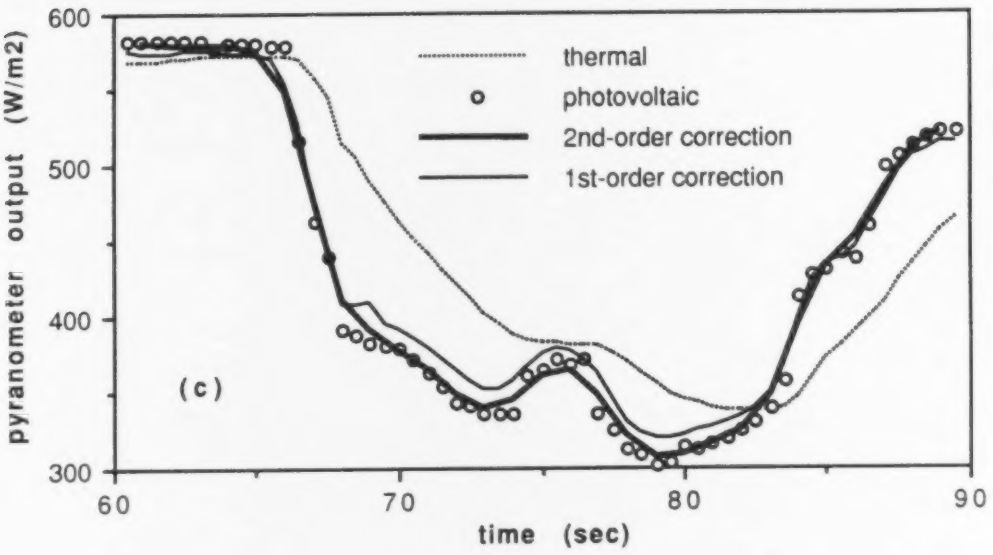

Figure 5.3 (Continued)

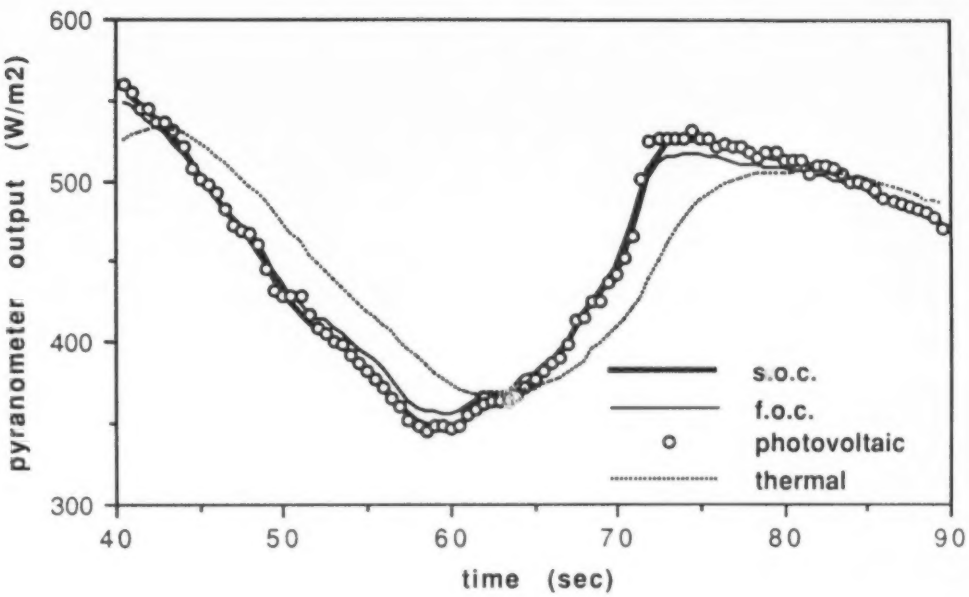

Figure 5.4 Demonstration of FOC and SOC in actual solar radiation measurement.

6. CONCLUSIONS

The major aim of this work is to measure and analyze the multi-exponential response phenomenon of thermal pyranometers. The purpose behind this aim is to correct the short term time response error produced by the relatively slow response of the conventional radiation measurement instruments. What is more interesting is that the correction scheme, developed in this work, may possibly be used for the correction of measured physical quantities that are the result of a dynamic process characterized by a transient function.

6.1 Summary of contributions

From a careful investigative study of the step response of CM-5 thermal pyranometers, it was found that the dynamic behavior of the radiation measurement instrument can be characterized by at least two response time constants. This appears to be the first report of such a second time constant having been measured and calculated quantitatively by numerically fitting the readings of the pyranometer subjected to a step radiation input. The measured values of the two time constants, under different physical and environmental conditions, show a good repeatability for each individual pyranometer. It can be concluded that the amplitudes of the two time constants, dominating over the dynamic behavior of CM-5 pyranometer, are independent of the spectral content and the intensity of incident radiation.

To simulate the double-exponential response, a double plate thermal model of the pyranometer has been developed and a transient function of the pyranometer input and output derived. Corresponding the two measured time constants (τ_1 and τ_2) to the transient function yields two of the three parameters in the function. In order to determine the remaining constant, a sinusoidal response experiment was performed using a simple sinusoidal radiation generator. Comparison between the experimental response with the theoretically calculated pyranometer frequency response determines the unknown constant.

Applying a fourth-order Runge-Kutta method, the transient equation was used to realize an error correction scheme with the capability of compensating the second order time response error of the pyranometer. The second order correction (SOC) demonstrated a definite improvement over the first order correction (FOC) in both laboratory experiments [17] and actual solar radiation measurements. With improved numerical techniques, real time compensation for time response error should be possible. In another words, the 'true' radiation value is able to be accurately anticipated before the thermal radiation sensor reaches its internal equilibrium. The SOC scheme is of great significance and importance for thermal pyranometers and pyrheliometers used in the instantaneous solar radiation measurements, as it improves the dynamic response of the instruments.

6.2 Limitations and suggestions for future work

The double plate thermal model for the pyranometer has given an

excellent explanation to the radiation behavior (response) of the thermal pyranometer, but it is not sufficient to characterize the thermal behavior of the instrument. The response of a thermal shock without incident radiation change can still be described by Equation (2.18) because no radiation change means the left hand side of Equation (2.17) is zero, as in the case of the step response. In a dark room (G=0), the condition of the thermal shock experiment, Equation (2.18) becomes:

$$G_i(t)=A\ \exp(-(t-t_0)/\tau_1)+B\ \exp(-(t-t_0)/\tau_2) \qquad (6.1)$$

Because no radiation exist in the experiment, the initial condition should be A+B=0 since $G_i=0$ at $t=t_0$. With this condition, a positive signal, shaped similarly to the testing result of Wardle and van den Brink [10, 11], will be generated from Equation (6.1) after the thermal shock occurs. If the values of τ_1 and τ_2 measured here, however, are substituted in (6.1), $G_i(t)$ occurs over a time period much shorter than observed in the thermal shock experiments (see Figure 1.4). This is because the instrument housing, which has a longer time constant, has isolated the thermal shock from the sensor plates. Further investigation on the housing effect would be needed in order to study the thermal shock phenomenon.

As mentioned before, the numerical differentiation algorithm used in SOC is the 5-point parabola fitting scheme, which 'looks ahead' $2\Delta t$ and $4\Delta t$ to yield the first and the second derivatives respectively. Thus a shortcoming of the method is that the consequent correction

often 'anticipates' some rapid change before it actually occurs [17]. Improvement on the numerical differentiation algorithm is therefore needed.

Limitation also appears in the sinusoidal response measurement. Due to the working principle of the system, the spectral content of the radiation was modulated as well as the intensity. Thus the spectral sensitivity of the photovoltaic pyranometer decreased the accuracy of the attenuation factor measurement. In addition to this, the range of the angular frequency is limited by the geometrical size of the sinusoidal modulator template and the driving wheel. The generated sinusoidal wave shape is imperfect due to the imperfect shape of the modulator template and the lamp filament image, both of which are not exactly the shapes assumed in Figure 4.2. A better sinusoidal radiation might be generated by letting the radiation beam go through two rotating polarized plates before reaching the pyranometer sensor. The angular frequency would be controlled by the rotating speed of the polarized plate.

Another aspect of a sinusoidal response measurement is that the frequency response of the sensor can be used to correct the time response error by the method of Fourier transform, provided the known frequency response range of the pyranometer is wide enough. Further work in this area will be needed in order to perform Fourier analysis in the instantaneous solar radiation measurement.

REFERENCES

[1] K.L. Coulson, Solar and terrestrial radiation, Academic Press, New York (1975)

[2] L.R. van Wely and G.J. van den Brink, Presentation of some of the IEA-instrument characteristics, *IEA Solar Heating and Cooling Programme Task IX Symposium*, D.I. Wardle and D.C. McKay, Eds., 95-105, Norrkoping (Jan. 1984)

[3] H. Suehrcke, The performance prediction of solar thermal systems, Ph.D. Thesis, University of Western Australia, Nedlands, Australia (1988)

[4] B.J. Brinkworth and T.D.R. Hughes, A method of obtaining fast response in solar pyranometers, *J. Phys. (E): Sci. Inst.* **8**, 902-903 (1975)

[5] B.J. Brinkworth and T.D.R. Hughes, Accelerated response of thermopile pyranometer, *Solar Energy* **18**, 403-404 (1976)

[6] H. Suehrcke, C.P. Ling and P.G. McCormick, The dynamic response of instruments measuring instantaneous solar radiation, *Solar Energy* **44**, 145-148 (1990)

[7] K. Dehne and R. Trapp, Preliminary report on the results of the first test loop of 4 pyranometers within IEA task IX, *IEA Solar Heating and Cooling Programme Task IX Symposium*, D.I. Wardle and D.C. McKay, Eds., 335-369, Norrkoping (Jan. 1984)

[8] P.M. Nast, Measurements of transients: irradiance, temperature, ageing, *IEA Solar Heating and Cooling Programme Task IX Symposium*, D.I. Wardle and D.C. McKay, Eds., 123-127, Norrkoping (Jan. 1984)

[9] L.J. Fritschen and L.W. Gay, Environmental instrumentation, Springer-Verlag, New York (1979)

[10] D.I. Wardle and D.V. Barton, Zero offsets in pyranometer signals related to long-wave radiation, temperature change and ventilation and some implications regarding measurement uncertainty. Internal Report ARDP 129X52, Environment Canada, Atmospheric Environment Service, (Feb. 1988)

[11] G.J. van den Brink, Preliminary presentation of characteristics of IEA pyranometers, *IEA Solar Heating and Cooling Programme Task IX Symposium*, D.I. Wardle and D.C. McKay, Eds., 371-387, Norrkoping (Jan. 1984)

[12] P.S. Acton, Numerical Methods that work, Harperand Row, New York (1970)

[13] B. Shen and A.M. Robinson, Response time measurement and analysis

of Kipp & Zonen CM-5 pyranometers, *Proceedings of 17th Annual Conference*, Solar Energy Society of Canada, pp. 331-334, 1991

[14] B. Shen and A.M. Robinson, Measurement and analysis of the step response of pyranometers requiring 2nd-order correction, *Solar Energy*, accepted for publication, September 1991

[15] Robert L. LaFara, Computer Methods for Science and Engineering, Hayden, New Jersey (1973)

[16] W.S. Dorn and D.D. McCracken, Numerical Methods with Fortran IV Case Studies, John Wiley & Sons, New York (1972)

[17] B. Shen and A.M. Robinson, Pyranometer frequency response measurement and general correction scheme for time response error, *Solar Energy*, accepted for publication, September 1991

[18] Jaroslav Pachner, Handbook of Numerical Analysis Applications, McGraw-Hill, New York (1984)

[19] C.J. Riordan, D.R. Myers and R.L. Hulstrom, Spectral solar radiation data base documentation, Solar Energy Research Institute, January 1990

APPENDIX A

PASCAL PROGRAM FOR DETERMINING THE BEST FIT FREQUENCY OF A SINUSOIDAL FUNCTION

```
  { Find the exact frequency of a trigonometric input - A:data.the }

type
  list = array[1..4000] of real;
var
  data,out: text;
  m,n,i,a1: integer;
  flag,res,res1,res2,w,w1,w2,shen,A,B,C,t,a0,a2,a3: real;
  b0,b1,b2,b3,c0,c1,c2,c3,dom,step: real;
  G: list;
begin
  write('Enter the initial Omega (rad/s): ');
  readln(w);
  write('Enter the sampling period (Seconds): ');
  readln(t);
  writeln('Enter the step change for Omega: ');
  readln(step);
  assign(data,'a:\data.the');
  m:=1;
  reset(data);
  while not eof(data) do
```

```
  begin
    readln(data,G[m]);
    m:=m+1;
  end;
a1:=m-1;
repeat
n:=0;
a2:=0;
a3:=0;
a0:=0;
b0:=0;
b2:=0;
b3:=0;
c0:=0;
c3:=0;
while n<a1 do
  begin
    a2:=a2+cos(w*n*t);
    a3:=a3+sin(w*n*t);
    a0:=a0+G[n+1];
    b2:=b2+sqr(cos(w*n*t));
    b3:=b3+cos(w*n*t)*sin(w*n*t);
    b0:=b0+G[n+1]*cos(w*n*t);
    c3:=c3+sqr(sin(w*n*t));
    c0:=c0+G[n+1]*sin(w*n*t);
    n:=n+1;
  end;
```

```
b1:=a2;
c1:=a3;
c2:=b3;
dom:=a1*(b2*c3-b3*c2)-a2*(b1*c3-b3*c1)+a3*(b1*c2-b2*c1);
A:=(a0*(b2*c3-b3*c2)-a2*(b0*c3-b3*c0)+a3*(b0*c2-b2*c0))/dom;
B:=(a1*(b0*c3-b3*c0)-a0*(b1*c3-b3*c1)+a3*(b1*c0-b0*c1))/dom;
C:=(a1*(b2*c0-b0*c2)-a2*(b1*c0-b0*c1)+a0*(b1*c2-b2*c1))/dom;
res:=0;
n:=1;
while n<a1+1 do
  begin
    res:=res+sqr(A+B*cos(w*(n-1)*t)+C*sin(w*(n-1)*t)-G[n]);
    n:=n+1;
  end;
writeln;
writeln('Current frequency (Omego) is:',w:6:5);
writeln('The residual is: ',res);
writeln;
w1:=w+step;
  n:=0;
a2:=0;
a3:=0;
a0:=0;
b0:=0;
b2:=0;
b3:=0;
c0:=0;
```

```
c3:=0;
while n<a1 do
  begin
    a2:=a2+cos(w1*n*t);
    a3:=a3+sin(w1*n*t);
    a0:=a0+G[n+1];
    b2:=b2+sqr(cos(w1*n*t));
    b3:=b3+cos(w1*n*t)*sin(w1*n*t);
    b0:=b0+G[n+1]*cos(w1*n*t);
    c3:=c3+sqr(sin(w1*n*t));
    c0:=c0+G[n+1]*sin(w1*n*t);
    n:=n+1;
  end;
  b1:=a2;
  c1:=a3;
  c2:=b3;
  dom:=a1*(b2*c3-b3*c2)-a2*(b1*c3-b3*c1)+a3*(b1*c2-b2*c1);
  A:=(a0*(b2*c3-b3*c2)-a2*(b0*c3-b3*c0)+a3*(b0*c2-b2*c0))/dom;
  B:=(a1*(b0*c3-b3*c0)-a0*(b1*c3-b3*c1)+a3*(b1*c0-b0*c1))/dom;
  C:=(a1*(b2*c0-b0*c2)-a2*(b1*c0-b0*c1)+a0*(b1*c2-b2*c1))/dom;
  res1:=0;
  n:=1;
  while n<a1+1 do
    begin
      res1:=res1+sqr(A+B*cos(w1*(n-1)*t)+C*sin(w1*(n-1)*t)-G[n]);
      n:=n+1;
    end;
```

```
    if res1<res then
      w2:=w1+step;
    if res1<res then
      flag:=1
    else
      begin
      w2:=w-step;
      flag:=-1
    end;
  n:=0;
  a2:=0;
  a3:=0;
  a0:=0;
  b0:=0;
  b2:=0;
  b3:=0;
  c0:=0;
  c3:=0;
  while n<a1 do
    begin
      a2:=a2+cos(w2*n*t);
      a3:=a3+sin(w2*n*t);
      a0:=a0+G[n+1];
      b2:=b2+sqr(cos(w2*n*t));
      b3:=b3+cos(w2*n*t)*sin(w2*n*t);
      b0:=b0+G[n+1]*cos(w2*n*t);
      c3:=c3+sqr(sin(w2*n*t));
```

```
    c0:=c0+G[n+1]*sin(w2*n*t);
    n:=n+1;
  end;
  b1:=a2;
  c1:=a3;
  c2:=b3;
  dom:=a1*(b2*c3-b3*c2)-a2*(b1*c3-b3*c1)+a3*(b1*c2-b2*c1);
  A:=(a0*(b2*c3-b3*c2)-a2*(b0*c3-b3*c0)+a3*(b0*c2-b2*c0))/dom;
  B:=(a1*(b0*c3-b3*c0)-a0*(b1*c3-b3*c1)+a3*(b1*c0-b0*c1))/dom;
  C:=(a1*(b2*c0-b0*c2)-a2*(b1*c0-b0*c1)+a0*(b1*c2-b2*c1))/dom;
  res2:=0;
  n:=1;
  while n<a1+1 do
    begin
      res2:=res2+sqr(A+B*cos(w2*(n-1)*t)+C*sin(w2*(n-1)*t)-G[n]);
      n:=n+1;
    end;
  if flag=1 then
    shen:=(res2-res1)*(res-res1);
  if flag=1 then
    w:=w1
  else
   begin
     shen:=(res2-res)*(res1-res);
     w:=w2;
   end;
until shen>0;
```

```
  if flag=-1 then
  w:=w+step;
  writeln('The exact frequency (Omega) is: ',w:6:5);
end.
```

APPENDIX B

PASCAL PROGRAM FOR 2ND ORDER TIME RESPONSE ERROR CORRECTION OF THERMAL PYRANOMETER

```
{
  This prgram is for the 2nd order correction of time response error
                        of thermal pyranometer.
    The instrument indicated readings are in the file--A:DATA.THE.
      The corrected reading will be given in file--A:BABY.DAT,
                        with the time label on.
}

type
  list1 = array[1..1000] of real;
  list2 = array[1..1000] of integer;
{
                          declare variables
}
var
  data,out: text;
  l,m,n,i,j,k: integer;
  t,t1,t2,c0,c1,c2,e,k1,k2,k3,k4: real;
  G,d1,d2,y:list1;
  cr: list2;
{
```

```
                    start the program
}
begin
{
          Enter the parameters of measurement and instrument
}
  write('Enter the sampling period: ');
  readln(t);
  write('Enter the two time constants: ');
  readln(t1,t2);
  c1:=t1*t2;
  c2:=t1+t2;
  write('Enter C0 of the transient function: ');
  readln(c0);
  write('Enter the Epsilon: ');
  readln(e);
{
                  input the pyranometer readings
}
  assign(data,'a:\data.the');
  m:=1;
  reset(data);
  while not eof(data) do
    begin
      readln(data,G[m]);
      m:=m+1;
    end;
```

```
  m:=m-1;
{
        calculate the 1st and 2nd derivatives of pyranometer
                        indicated radiation
}
  d1[1]:=(-21*G[1]+13*G[2]+17*G[3]-9*G[4])/20/t;
  d1[2]:=(-11*G[1]+3*G[2]+7*G[3]+G[4])/20/t;
  d1[m-1]:=(11*G[m]-3*G[m-1]-7*G[m-2]-G[m-3])/20/t;
  d1[m]:=(21*G[m]-13*G[m-1]-17*G[m-2]+9*G[m-3])/20/t;
  n:=3;
  while n<m-1 do
    begin
      d1[n]:=(-2*G[n-2]-G[n-1]+G[n+1]+2*G[n+2])/10/t;
      n:=n+1;
    end;
  d2[1]:=(-21*d1[1]+13*d1[2]+17*d1[3]-9*d1[4])/20/t;
  d2[2]:=(-11*d1[1]+3*d1[2]+7*d1[3]+d1[4])/20/t;
  d2[m-1]:=(11*d1[m]-3*d1[m-1]-7*d1[m-2]-d1[m-3])/20/t;
  d2[m]:=(21*d1[m]-13*d1[m-1]-17*d1[m-2]+9*d1[m-3])/20/t;
  n:=3;
  while n<m-1 do
    begin
      d2[n]:=(-2*d1[n-2]-d1[n-1]+d1[n+1]+2*d1[n+2])/10/t;
      n:=n+1;
    end;
{
        determine the refreshing points for the initial value
```

```
}
  j:=1;
  i:=1;
  while i<m do
  begin
    if abs(d1[i])+abs(d2[i])>e then
      i:=i+1
      else
       begin
        cr[j]:=i;
        i:=i+1;
        j:=j+1;
       end;
  end;
  cr[j]:=m;
{
              give warning if no refreshing point found
}
  if j=1 then
   writeln('No correction performed because Epsilon is too small!')
{
                       start error compensation
}
  else
   begin
    write('Correction starts after',cr[1]*t,'seconds. ');
   end;
```

```
  k:=1;
  while k<j do
   begin
    n:=cr[k];
    l:=cr[k];
    y[l]:=G[l];
    while n<cr[k+1] do
      begin
       k1:=(c1*d2[n]+c2*d1[n]+G[n]-y[l])/c0;
       k2:=(c1*d2[n+1]+c2*d1[n+1]+G[n+1]-(y[l]+t*k1))/c0;
       k3:=(c1*d2[n+1]+c2*d1[n+1]+G[n+1]-(y[l]+t*k2))/c0;
       k4:=(c1*d2[n+2]+c2*d1[n+2]+G[n+2]-(y[l]+2*t*k3))/c0;
       y[l+2]:=y[l]+t*(k1+2*k2+2*k3+k4)/3;
       y[l+1]:=(y[l]+y[l+2])/2;
       l:=l+2;
       n:=n+2;
      end;
    k:=k+1;
  end;
{
                    output the corrected values
}
  assign(out, 'a:\baby.dat');
  rewrite(out);
  n:=cr[1];
  while n<m+7 do
    begin
```

```
        writeln(out,n*t,' ',y[n]);
        n:=n+1;
      end;
end.
```